

Acknowledgments. We wish to thank the referees, listed below, for the countless hours they devoted to critical review of the papers appearing in the two volumes: K. A. Anderson, T. P. Armstrong, A. Barnes, L. F. Burlaga, D. C. Ellison, D. H. Fairfield, M. A. Forman, D. W. Forslund, R. W. Fredricks, B. E. Goldstein, M. L. Goldstein, J. T. Gosling, E. W. Greenstadt, C. A. Gurgiolo, T. Hada, J. D. Huba, M. K. Hudson, J. R. Kan, P. J. Kellogg, A. J. Lazarus, M. A. Lee, R. P. Lepping, R. P. Lin, W. H. Matthaeus, K. Papadopoulos, G. K. Parks, G. Paschmann, K. B. Quest, P. Rodriguez, C. T. Russell, F. L. Scarf, J. D. Scudder, D. D. Sentman, N. R. Sheeley, Jr., G. L. Siscoe, E. J. Smith, S. S. Stahara, S. T. Suess, J. A. Van Allen, K. P. Wenzel, R. T. Woo, and C. S. Wu. The Chapman conference, held in Napa, California, February 20–24, 1984, and these books owe a major portion of their success to the tireless efforts of Christina Brokl of the Jet Propulsion Laboratory and Barbara Holland of the Goddard Space Flight Center. These books could not have been possible without the support of the National Science Foundation and the National Aeronautics and Space Administration and, in particular, the moral and financial support of the International-Sun-Earth-Explorer Project. We also wish to express our special appreciation to the American Geophysical Union's publication staff, who provided exceptional management support throughout this endeavor.

ROBERT G. STONE
*NASA Goddard Space Flight Center
Greenbelt, Maryland*

BRUCE T. TSURUTANI
*Jet Propulsion Laboratory
California Institute of Technology
Pasadena*

A Quarter Century of Collisionless Shock Research

C. F. KENNEL

*Department of Physics, Institute for Geophysics and Planetary Physics, and Center for Plasma Physics and Fusion Engineering
University of California, Los Angeles, California 90024*

J. P. EDMISTON AND T. HADA

*Department of Physics and Institute for Geophysics and Planetary Physics
University of California, Los Angeles, California 90024*

This review highlights conceptual issues that have both governed and reflected the direction of collisionless shock research in the past quarter century. These include MHD waves and their steepening, the MHD Rankine-Hugoniot relations, the supercritical shock transition, nonlinear oscillatory wave trains, ion sound anomalous resistivity and the resistive-dispersive transition for subcritical shocks, ion reflection and the structure of supercritical quasi-perpendicular shocks, the earth's foreshock, quasi-parallel shocks, and, finally, shock acceleration processes.

1. Introduction

Twenty-five years ago it was hotly debated whether collisionless shock waves even existed. Some argued that the rarity of collisions in a high-temperature plasma precluded the existence of shocks, while others maintained that collective microturbulence would replace particle collisions to create a shock with a thickness much less than a collision mean free path. The solar wind proved, upon its discovery in 1960, to have an enormous mean free path—comparable to the distance from the earth to the sun—yet the rapid rise times of the sudden commencements initiating magnetic storms suggested that solar flare plasma injection did create a thin collisionless shock (T. Gold (1955) cited by Sagdeev [1979]) [Levy *et al.*, 1964]. Since it had been difficult to make collision-free plasmas in the laboratory, some foresaw that the first truly collisionless shock would be discovered in space. And so it was, standing in the solar wind ahead of the earth's magnetosphere [Sonett and Abrams, 1963; Ness *et al.*, 1964].

The following decade (1964–1974) was a golden age of collisionless shock research. The study of nonlinear collective plasma processes was in its infancy as the golden age opened, and collisionless shocks were the simplest example that illuminated the self-regulating interrelationship between macroscopic flows and microscopic

collective processes that is central to most plasma configurations. High-altitude nuclear weapons studies and magnetic pinch fusion research motivated major laboratory investigations of collisionless shocks in the United States, Europe, and the Soviet Union. The discovery of the earth's bow shock ensured that space observations would play a major role in collisionless shock research. Some of the first numerical simulations were of collisionless shocks. There was a marvelous collaboration between laboratory and space experimentalists, theorists, and specialists in numerical simulation.

The marvelous collaboration ended suddenly in 1974, largely because financial support for laboratory experiments disappeared when interest in magnetic pinch fusion waned. The space community was left to its own devices. Actually, because space plasmas are collision free and boundary free, and because the quality and variety of space plasma data were increasing rapidly, the space community was beginning to assert its dominance in collisionless shock research even before laboratory activity ceased.

The major achievement of the bridge years between the first and second golden ages, 1974–1979, was a phenomenological classification of the dependence of the earth's bow shock structure on upstream solar wind parameters which revealed a richness of shock structure that did not

and could not emerge from the limited number of laboratory experiments that had been performed.

The ISEE spacecraft program initiated a second golden age of shock research, which began in 1979–1980 when detailed analyses of the earth's bow shock data started to appear in the literature. The ISEE program is well suited to bow shock studies; the use of two spacecraft makes it possible to measure scale lengths, easy to do in the laboratory but difficult in space, and the ISEE plasma diagnostics far exceed the previous laboratory standards of accuracy and completeness. A new generation of numerical simulations was stimulated by the new space measurements, and previously independent research on shock structure and the acceleration of particles by shocks began to converge.

We do not intend to repeat other detailed reviews of early collisionless shock research [Tidman and Krall, 1971; Biskamp, 1973; Formisano, 1977; Sagdeev, 1979; Greenstadt and Fredricks, 1979; Eiselevich, 1982, 1983] or the comprehensive review of our present knowledge by Greenstadt et al. [1984]. We will not attempt to apportion research credit. Rather, we will highlight conceptual issues that have both governed and reflected the direction of collisionless shock research in the past quarter century.

The first six sections discuss fluid theories of shock structure, a natural starting point, and the main success of the first golden age. Sagdeev [1979] has reviewed the theory of collisionless shocks in unmagnetized plasmas; we will consider only the magnetized case. Section 2 begins by defining the three small-amplitude magnetohydrodynamic waves which determine the characteristics along which information about boundary conditions is propagated in magnetohydrodynamic flows. Viewing them as shocks of infinitesimal amplitude illustrates what changes in plasma properties propagate along which characteristics, shows how fast and slow compressional waves steepen to form shocks, and illuminates the properties of finite amplitude shocks. Considerations of shock evolution or steepening, which follow naturally from the use of fluid theory, eliminate certain extraneous solutions to the MHD Rankine-Hugoniot conditions (section 3), explain the formation of dissipative subshocks (section 4) and dispersive wave trains (section 5), and define the transition between dissipative and dispersive structure in shocks with ion sound anomalous resistance (section 6).

Section 4 discusses the structure of fast shocks predicted by dissipative MHD theory. Here one important result has survived: the identification of a critical Mach number above which the dissipation can no longer be exclusively due to resistivity. Shock steepening arguments indicate that the critical Mach number is defined for all upstream plasma parameters by the condition that the downstream flow speed equal the sound speed. Section 4 closes with a numerical calculation of the sensitive dependence of the critical Mach number on upstream

plasma parameters, which even today is not widely appreciated.

Section 5 deals with dispersive shocks, in which a nonlinear oscillatory wave train accomplishes the shock transition. The basic features of finite amplitude wave trains can be estimated from the properties of the corresponding small-amplitude waves described by the two-fluid approximation. We will show that dispersive wave trains have the same critical Mach number as laminar resistive shocks. Whether a resistive or dispersive subcritical shock will form can be determined once the ratio of the resistive to dispersive scale lengths is known.

The ion sound instability has long been a candidate for anomalous resistance in weakly magnetized plasmas like the solar wind, and its saturation has been well understood since the early 1970s [Galeev, 1976]. In section 6, we review the properties of ion sound anomalous resistance in the quasi-linear regime most pertinent to bow shock measurements. Steepening arguments indicate that equating the dispersive and ion sound resistive scale lengths defines the parameters for which a subcritical shock changes from resistive to dispersive. Only recently have enough observations of subcritical bow shocks been gathered to test this approach.

The classical treatment of collisionless shock structure started with the fluid approximation. The primary concession it made to the kinetic nature of plasmas was to recognize the difference between the ion and electron inertial responses by using two-fluid theory. To allow for dissipation, artificial collision frequencies were inserted in the fluid equations, whose solutions then defined how and when microinstabilities could grow in the shock front. Knowing how a particular brand of microturbulence saturated, one then estimated the turbulent dissipation coefficients, and the "anomalous" collision frequencies, and tested the consistency of the fluid and kinetic level calculations.

Underlying the classical approach were two often unstated assumptions: first, that plasma dissipation is local and diffusive as the fluid model presumes, and, more important, that microturbulence is the only kinetic effect pertinent to shocks. This philosophy appears to be useful primarily for subcritical shocks, which are a minor fraction of the bow shocks observed in space. More modern theoretical research, which has been guided exclusively by space observations, has therefore gone beyond the fluid approach. It has proven fruitful to partition the plasma ions into separate phase space classes according to how they interact with the shock. Reflected ions control the structure of supercritical quasi-perpendicular shocks, which we discuss in section 7. The fluid theory assumption that ion heat flows are negligible breaks down for quasi-parallel shocks (section 9), in which the interaction between low-energy plasma and superthermal ions energized by their interaction with the shock is a central structural feature.

Essential to supercritical and quasi-parallel shock

physics is the realization that not all ions are bound into a single fluid by microturbulence. Although the highly structured ion distributions occurring in such shocks may be unstable, the fluctuations produced by the instabilities are often secondary to free-streaming effects and provide primarily a means by which complete thermodynamic equilibrium may be reached. When different regions of phase space behave differently, the classical causality arguments, which were based on the existence of unique signal speeds in fluid theory, are no longer completely trustworthy. No longer must a shock steepen to provide the added dissipation required as its Mach number increases. In fact, the long mean free paths of the superthermal ions generated by supercritical and quasi-parallel shocks imply that shocks thicken outside the regime for which simple fluid theory is adequate.

By the early 1970s no laboratory experiment could match the range of plasma parameters that had been provided for free by the variable solar wind. A spacecraft experimentalist with imagination, a sense for geometry, cooperative colleagues, and patience could win hands down over his laboratory competitors. His advantage would have been far less striking were shock structure not as parameter sensitive as it turned out to be. In retrospect, many early disagreements about the bow shock—whether it was thick or thin, for example—occurred because we were slow to appreciate how parameter-dependent collisionless shocks really are. Eventually, a large international effort produced a classification of the dependence of bow shock magnetic structure upon upstream solar wind parameters (section 8), which revealed the profound difference between thin quasi-perpendicular shocks and thick quasi-parallel shocks. Quasi-parallel shocks are so thick that they could not have been found in the early laboratory experiments, and modern simulations must be carefully designed to contain the large spatial scales which characterize them. Their discovery is the most fundamental achievement of bow shock research.

The space community also consolidated numerous individual investigations of the region upstream of the earth's bow shock into a unified phenomenological picture that motivates much of today's research (section 8). Because of the unexpectedly large spatial scale of the quasi-parallel shock, this picture must explicitly take into account the facts that the bow shock is three dimensional, curved, and of finite extent. The most important new conception arising from this research was that of the "foreshock" [Greenstadt, 1975], which not only organizes the observations of upstream waves and particles, but also links bow shock observations directly to models of particle acceleration.

In recent years, the space plasma, cosmic ray, and astrophysical plasma physics communities have been occupied with different aspects of three general questions:

1. How does collisionless shock structure depend on upstream plasma parameters? In particular, why are

quasi-parallel and quasi-perpendicular shocks so different?

2. How do collisionless shocks accelerate particles to high energies?

3. How does energetic particle acceleration affect shock structure?

It is gradually becoming clear that all three questions are interrelated, and, as a result, fruitful interchanges between those interested in collisionless shock structure, particle acceleration, and cosmic ray physics are beginning to take place.

Although theoretical models of quasi-parallel shocks (section 9) are over 20 years old, and although the suggestion that energetic particles are significant to shock structure is equally venerable, experimentalists could do little with these ideas until recently. The earth's foreshock has a complex phenomenology whose disorder had to be reduced before it could be fitted into a theoretical framework that had once seemed ill adapted to bow shock observations. Moreover, quasi-parallel shocks have such enormous spatial scale that it now seems better to use interplanetary shocks to test theories of their structure.

A coherent viewpoint is now emerging from the research of the past 5 years (section 10). Recent observations of waves and energetic particles associated with interplanetary shocks also reveal the difference between the quasi-perpendicular and quasi-parallel parameter regimes found earlier in bow shock studies. Only quasi-parallel shocks have foreshocks containing magnetohydrodynamic turbulence upstream that is the essential ingredient for first-order Fermi acceleration. It appears that superthermal and energetic particles can stream relatively freely through quasi-parallel shocks, and that these particles generate the wave fields that scatter them. The outlines of a theory that will eventually predict the intensity and spectrum of accelerated particles as a function of shock parameters and time evolution are in view.

2. Small-Amplitude MHD Waves

2.1. Basic Properties

Ideal magnetohydrodynamic theory consists of equations for the conservation of mass, momentum, and specific entropy, Faraday's law of magnetic induction together with the "frozen in field" assumption, and $\nabla \cdot \mathbf{B} = 0$. Because these equations are free of dissipation and dispersion, they cannot describe the processes that form shock structure, but they do describe small-amplitude long-wavelength waves, the steepening of these waves to discontinuities, and the changes in plasma state that must take place across the discontinuities.

Linearizing the ideal MHD equations about an infinite homogeneous equilibrium leads to three small-amplitude plane waves, whose phase speeds depend upon the angle θ of their propagation to the magnetic field, \mathbf{B} , and the

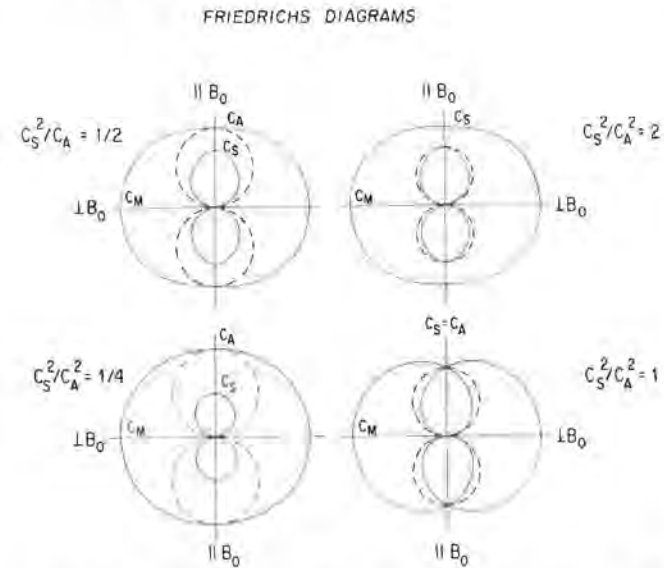


Fig. 1. MHD Friedrichs diagrams. The Friedrichs diagram displays the dependence of the 3 MHD plane wave speeds (radial coordinate) on their angle of propagation to the magnetic field (angular coordinate) in a polar plot whose vertical axis is parallel to the magnetic field. Four cases are shown, with $C_s^2/C_A^2 = \frac{1}{4}$ and $\frac{1}{2}$ in the left-hand column and $C_s^2/C_A^2 = 1$ and 2 in the right. C_s and C_A are the sound and Alfvén speeds, respectively. The fast and slow waves, which steepen, are indicated by solid lines, while the intermediate wave, which does not steepen, is indicated by a dashed line. The magnetosonic wave propagates perpendicular to the magnetic field with the speed $C_M = (C_s^2 + C_A^2)^{1/2}$. For parallel propagation, the fast and intermediate speeds equal the Alfvén speed when $C_s^2/C_A^2 < 1$, while the slow and intermediate speeds equal the Alfvén speed when $C_s^2/C_A^2 > 1$. When $C_s^2/C_A^2 = 1$, all three speeds are equal.

sound and Alfvén speeds, C_s and C_A , respectively, where

$$C_s^2 = \gamma P/\rho \quad C_A^2 = B^2/4\pi\rho \quad (1)$$

and P , ρ , and γ are the plasma pressure, mass density, and ratio of specific heats. The three MHD waves are ordered by their speeds, which are called fast, intermediate, and slow (C_F , C_I , and C_{SL} , respectively), where

$$C_I^2 = C_A^2 \cos^2 \theta \quad (2)$$

$$C_F^2 = \frac{1}{2} \{ (C_A^2 + C_s^2) \pm [(C_A^2 + C_s^2)^2 - 4C_A^2 C_s^2 \cos^2 \theta]^{1/2} \} \quad (3)$$

By defining the fast mode to have the larger of the two speeds in (3), it follows that $C_F \geq C_I \geq C_{SL}$ for all θ , C_s , and C_A .

For propagation perpendicular to the magnetic field ($\theta = 90^\circ$), (2) and (3) reduce to

$$C_I = C_{SL} = 0 \quad C_F = (C_A^2 + C_s^2)^{1/2} \equiv C_M \quad (4)$$

so that only one wave, the magnetosonic wave, propagates with a nonzero speed. For parallel propagation

($\theta = 0^\circ$), (2) and (3) indicate that when $C_A > C_s$, the fast and intermediate speeds are identical, whereas when $C_s > C_A$, the intermediate and slow speeds are equal. For all other angles of propagation, the three MHD speeds are distinct.

The dependences of the MHD wave speeds upon the propagation angle θ may be visualized with the aid of a Friedrichs diagram, a two-dimensional polar plot whose radial coordinate is the wave speed and whose polar angle is the angle θ . Figure 1 shows four Friedrichs diagrams adapted from *Kantrowitz and Petschek* [1966], for $C_s^2/C_A^2 = \frac{1}{4}$, $\frac{1}{2}$, 1 , and 2 . The vertical axes are parallel to the magnetic field. The fast and slow modes are indicated by solid lines and the intermediate mode by dashed lines.

Since ideal MHD contains no fundamental scale length, the MHD wave speeds are independent of wavelength, and small-amplitude discontinuities as well as periodic waves obey the linearized MHD equations. Such step waves, shocks of infinitesimal amplitude, describe how changes in plasma properties propagate along MHD characteristics. According to *Kantrowitz and Petschek* [1966]:

1. The fluid velocity increments across the fast, intermediate, and slow waves are mutually perpendicular.
2. For fast and slow waves, both the velocity and the magnetic field remain in the plane defined by the magnetic field ahead of the wave and the wave normal. This coplanarity property, which is preserved for finite amplitude fast and slow shocks, is often used to determine the shock normal from spacecraft data.
3. For the fast (slow) mode, the magnetic pressure increases (decreases) when the density increases. When the density decreases, the magnetic pressure decreases (increases) across a fast (slow) mode.
4. The intermediate wave rotates the magnetic field and fluid velocity out of the coplanarity plane without changing any other plasma property.

Properties 1–4 above also apply to finite amplitude discontinuities.

2.2. Wave Steepening

Imagine that a piston generates two successive infinitesimal shocks in the same mode. We may determine whether nonlinear isentropic MHD waves steepen simply by asking whether the trailing wave overtakes the leading wave. Their speeds differ because the leading wave changes the Alfvén, sound, and fluid speeds. A compressional wave increases the fluid speed in the stationary frame—the principal effect that enables the trailing wave to catch the leading wave [*Petschek*, 1958].

Fast and slow waves steepen when [*Kantrowitz and Petschek*, 1966]

$$\frac{\rho}{C} \frac{\delta(U+C)}{\delta\rho} = 1 + \frac{1}{2} \frac{(\gamma-1)C_A^2 C_s^2 \sin^2 \theta + (C^2 - C_s^2)^2}{C_A^2 C_s^2 \sin^2 \theta + (C^2 - C_s^2)^2} > 0 \quad (5)$$

In (5), $\delta(U+C)$ is the speed of the second wave relative to the first, U is the fluid velocity component parallel to the wave normal, and C is the wave speed relative to the fluid (either fast or slow). The expression (5) is always positive, so that compressional waves ($\delta\rho > 0$) steepen. By resolving a smooth pressure pulse into a number of small-amplitude step waves, we infer that the compressional parts of the pulse steepen, while its rarefactive portions separate. Intermediate waves do not steepen, because they do not alter the density, the normal component of the flow speed, or the Alfvén and sound speeds.

The quantity $\delta(U+C)/C$ in (5) may also be interpreted as the ratio of the steepening rate, $\gamma_s = k\delta(U+C)$, to the frequency, $\omega = kC$, of a periodic fast or slow wave of a given density amplitude, $\delta\rho/\rho$. The normalized fast (solid) and slow (dotted) mode steepening rates are plotted in a Friedrichs diagram format in the top row of Figure 2 for $C_s^2/C_A^2 = 0.3$, 1 , and 3 , assuming $\delta\rho/\rho = 1$. The exact steepening rates may be obtained by dividing the quantities in Figure 2 by $\delta\rho/\rho$. For a given $\delta\rho/\rho$, the fast and slow steepening rates are roughly independent of propagation angle, are almost equal for all C_s^2/C_A^2 , and are identical for $C_s^2/C_A^2 = 1$.

Because parallel fast and slow waves do not change the density when $C_s^2/C_A^2 < 1$ and $C_s^2/C_A^2 > 1$, respectively, it is more illuminating to derive the expressions analogous to (5) for a given perturbed fluid speed, $\delta|V|$, or, better yet, for a given perturbed energy density. The second and third rows of Figure 2, which show the steepening rates for $\delta|V| = (C_A^2 + C_s^2)^{1/2}$ and δ (energy density) $= \frac{1}{2} \rho(C_A^2 + C_s^2)$, respectively, indicate that parallel fast modes do not steepen when $C_s^2/C_A^2 < 1$ and that parallel slow modes do not steepen when $C_s^2/C_A^2 > 1$.

In order that nonlinear waves actually steepen, the above fluid steepening rates must exceed the wave damping rates calculated from kinetic theory. For the solar wind conditions prevailing at 1 AU, fast waves will nearly always steepen, whereas slow waves of comparable energy density will steepen only if the ion β is very low [*Hada and Kennel*, 1985].

3. MHD Rankine-Hugoniot Relations

3.1. Introduction

A nonlinear pressure pulse steepens until there is sufficient dissipation to form a steady shock. The structure of the dissipation layer is not describable by ideal MHD. However, the stationary states asymptotically far upstream and downstream of the shock are spatially uniform and therefore free of dissipation. As a result, ideal MHD does describe the change in flow parameters between the two stationary states provided that the specific entropy is allowed to increase. These jump conditions, the MHD Rankine-Hugoniot (RH) relations, are obtained by integrating the MHD conservation laws (with an equation for conservation of energy replacing that for

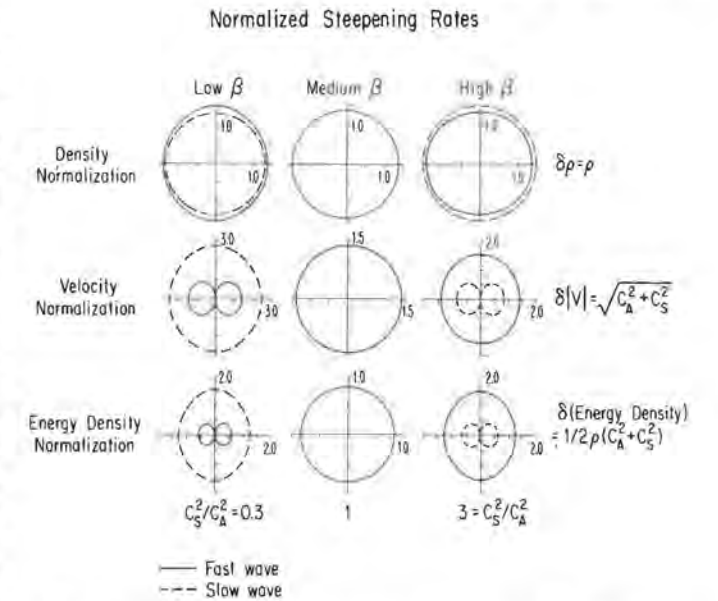


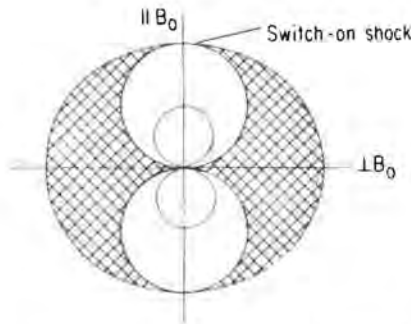
Fig. 2. Normalized MHD wave steepening rates. The normalized steepening rate defined in equation (8) is displayed in a polar plot for $C_s^2/C_A^2 = 0.3$, 1 , and 3 , and $\gamma = \frac{5}{3}$ in the top row. The vertical and horizontal axes are parallel and perpendicular to the magnetic field, respectively. The fast and slow mode steepening rates are indicated by solid and dashed lines, respectively. The steepening rates for step waves with $\delta\rho = \rho$ are shown; these may be adjusted to any given density amplitude by dividing by $\delta\rho/\rho$. When $C_s^2/C_A^2 < 1$, the fast mode steepens faster than the slow wave, and vice versa when $C_s^2/C_A^2 > 1$. The two steepening rates are equal when $C_s^2/C_A^2 = 1$. The parallel propagating fast and slow waves do not perturb the density when $C_s^2/C_A^2 < 1$ and $C_s^2/C_A^2 > 1$ respectively, and therefore do not steepen. It is more illuminating to plot the steepening rates for a velocity perturbation equal to the magnetosonic speed (middle row) or for a perturbed energy density equal to $1/2 \rho C_M^2$ (bottom row).

entropy) across the shock, which is considered to be discontinuity [*DeHoffman and Teller*, 1950].

There are fast and slow shocks, and an intermediate wave or rotational discontinuity, which neither steepens nor changes the specific entropy. Shocks are always compressional. This conclusion, which is consistent with the fact that only compressional waves steepen, does not follow automatically from the formal RH relations, whose solutions correspond to the flow going from low to high density or vice versa. However, since the specific entropy is higher on the higher-density side of the discontinuity, the density must always increase across a shock.

The shock frame flow velocity upstream of a fast (slow) shock is greater than the fast (slow) wave speed upstream and less than the fast (slow) speed downstream. This statement can be made plausible by using evolutionary arguments. Let us imagine a shock to evolve from a steepening pressure pulse, which we divide into a number of small-amplitude step waves. As the first few compressional

ALLOWED DOWNSTREAM FLOW SPEEDS FOR FAST SHOCKS



ALLOWED UPSTREAM FLOW SPEEDS FOR SLOW SHOCKS

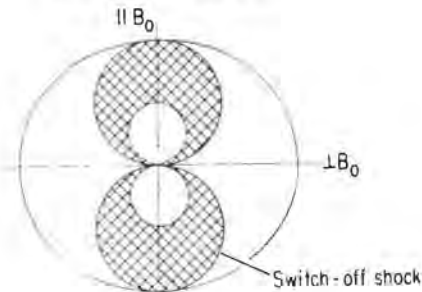


Fig. 3. MHD shock evolutionary conditions. The top and bottom panels show a $C_s^2/C_A^2 = \frac{1}{2}$ Friedrichs diagram of the fast, intermediate, and slow wave speeds. A fast shock takes the normal component of the shock frame flow speed from above the fast speed upstream to between the fast and intermediate speeds downstream. A slow shock takes the flow speed from between the slow and intermediate speeds upstream to below the slow speed downstream. For parallel propagation, the fast and intermediate speeds equal the Alfvén speed when $C_s^2/C_A^2 < 1$. If $C_s^2 < C_A^2$ downstream, the normal component of the flow speed must equal the Alfvén speed. In this case, the shock "switches on" a tangential component of magnetic field and flow speed. Switch-on shocks occur when $C_s^2 < C_A^2$ upstream and the fast Mach number is less than or equal to 2. For the maximum strength slow shock, the flow speed equals the intermediate speed upstream. This shock "switches off" the tangential component of the magnetic field downstream.

sion waves cross, the shock forms, and subsequent waves strengthen the shock until dissipation balances steepening.

In order that the pressure pulses overtake the shock, the flow speed must be smaller than the fast (slow) wave speed downstream. On the other hand, if the flow speed upstream were less than the fast (slow) speed, compressional waves would run ahead from downstream, and the shock profile would be unsteady.

The Rankine-Hugoniot relations contain extraneous solutions that take the normal component of the shock frame flow speed from above to below the intermediate speed. Evolutionary arguments indicate that when the

boundary conditions demand such a flow configuration, an additional finite amplitude intermediate wave must be inserted in the flow [Kantrowitz and Petschek, 1966]. Thus, the shock frame flow speed must exceed the intermediate speed downstream of a fast shock, and it cannot exceed the intermediate speed upstream of a slow shock. The regions of allowed flow speeds are shaded in the $C_s^2 = 1/4 C_A^2$ Friedrichs diagram of Figure 3.

The maximum strength slow shock switches off the tangential magnetic field component downstream. It occurs when the upstream flow speed equals the intermediate speed and is called the "switch-off" shock. For

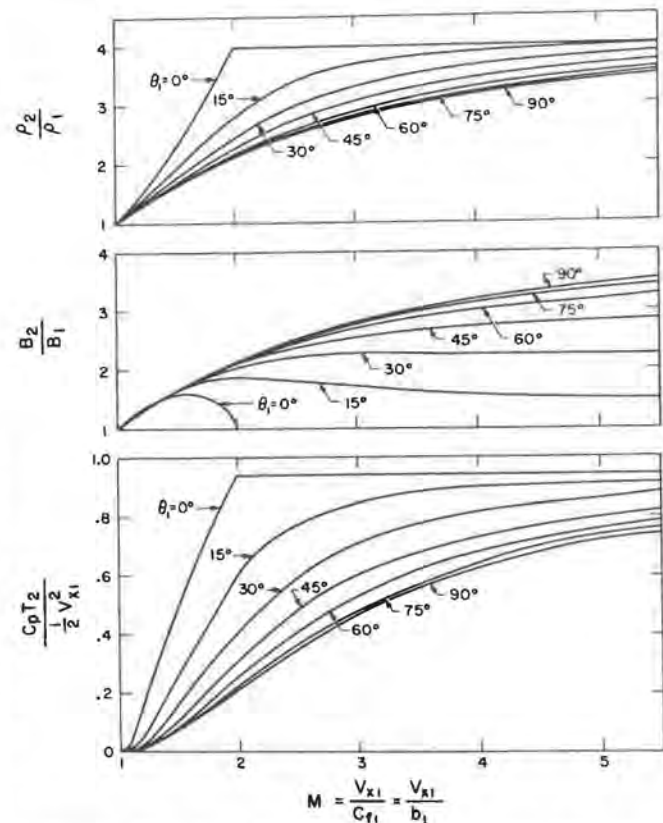


Fig. 4. Fast shock Rankine Hugoniot solutions for $C_s^2 = 0$ upstream. The density compression ratio (top), the magnetic field compression ratio (middle), and the ratio of the downstream internal energy density to the upstream flow energy density (bottom) are plotted as a function of the fast Mach number M assuming $\gamma = \frac{5}{3}$. The solutions for shock normal angles (denoted in this figure by θ_1) in 15° intervals from 0° to 90° are shown. The discontinuous change at $\theta_1 = 0$ and $M = 2$ is due to the disappearance of the switch-on shock. Above $M = 2$, B_2/B_1 is unity, and the density compression ratio and normalized internal energy density equal their strong shock limits of 4 and $\frac{13}{8}$ respectively. The more oblique the shock, the higher the Mach number at which it approaches the strong shock limit. The RH solutions depend weakly on shock normal angle for $45^\circ < \theta_1 \leq 90^\circ$. Thus, quasi-parallel ($\theta_1 < 45^\circ$) and quasi-perpendicular ($\theta_1 > 45^\circ$) shocks differ considerably. This figure is from Kantrowitz and Petschek [1966].

MHD RANKINE-HUGONIOT SOLUTIONS

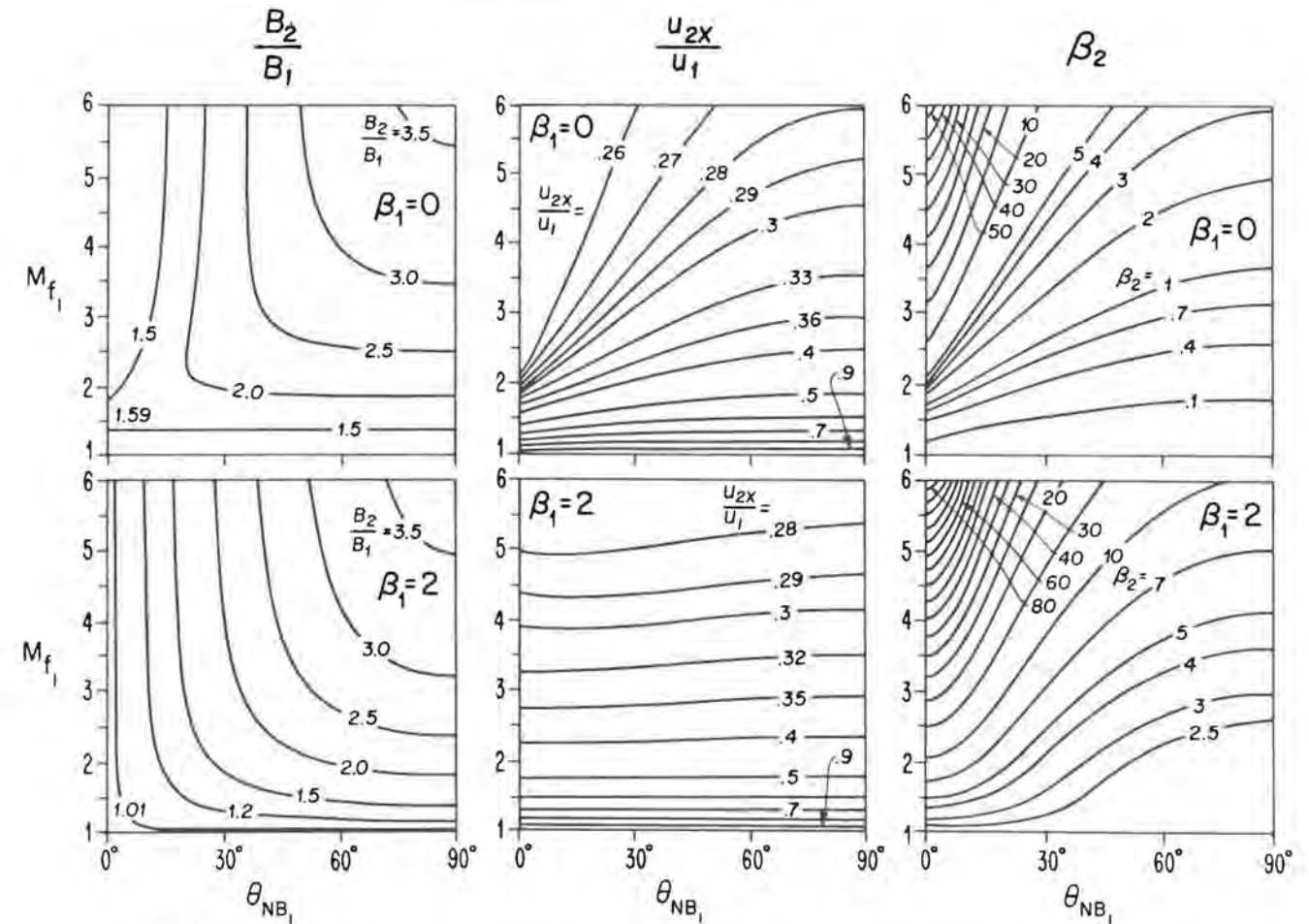


Fig. 5. Fast shock Rankine-Hugoniot solutions. The magnetic field compression ratio (left column), the velocity contrast (the inverse of the density compression ratio, middle column), and the downstream β_2 (right column) are contoured as functions of fast Mach number M_{f1} (vertical axes) and upstream shock normal angle θ_{NB1} (horizontal axes) for upstream $\beta_1 = 0$ (top row) and $\beta_1 = 2$ (bottom row). The quantity β is the ratio of thermal to magnetic pressure. It is interesting to contrast parallel and perpendicular shocks for low and high β_1 .

$C_s^2 < C_A^2$ and $\theta = 0^\circ$ the fast and intermediate speeds are identical; if $C_s^2 < C_A^2$ downstream of a parallel fast shock, the evolutionary conditions demand that the normal component of the downstream flow velocity precisely equal the intermediate speed. To accomplish this, parallel fast shocks "switch-on" tangential components of flow velocity and magnetic field downstream when the fast Mach number is less than 2 and $C_s^2 < C_A^2$ upstream. Such shocks are called "switch-on" shocks.

3.2. Numerical Rankine-Hugoniot Solutions for Fast Shocks

The Rankine-Hugoniot relations calculate the dependence of the downstream flow state on the upstream flow speed or Mach number, the ratio of the sound to Alfvén

speeds upstream (or, equivalently, the ratio of the thermal and magnetic pressures, β_1), and the shock normal angle. Although it is sometimes convenient experimentally to specify the Alfvén or magnetosonic Mach numbers, the steepening argument indicates that the physically rigorous parameter is the fast Mach number, the ratio of the upstream flow speed to the upstream fast speed based upon the shock normal angle.

Figure 4, from Kantrowitz and Petschek [1966], shows the dependences on the fast Mach number and shock normal angle of the density compression ratio ρ_2/ρ_1 , the magnetic field compression ratio B_2/B_1 , and the flow internal energy (enthalpy) downstream of shocks that propagate into a cold plasma ($\beta_1 = 0$) whose ratio of specific heats, γ , is $\frac{5}{3}$. As the fast Mach number approaches infinity

ty, the density and magnetic compression ratios approach a limit of 4 for all shock normal angles. In general, it may be shown that ρ_2/ρ_1 and B_2/B_1 approach $\gamma + 1/\gamma - 1$ and the downstream internal energy density approaches $\frac{1}{2}$ of the upstream flow energy density (when $\gamma = \frac{5}{3}$) in the strong shock limit.

The complex structure for fast Mach numbers less than 2 and nearly parallel propagation in Figure 4 is due to the switch-on shock. When $C_s^2 > C_A^2$ upstream, or when the Mach number exceeds 2, switch-on shocks no longer exist, and this structure disappears.

The three columns of Figure 5 contour the dependences on the fast Mach number, M_{f1} , and the upstream shock normal angle of the magnetic compression ratio (left column), the velocity contrast (middle column), and the ratio β_2 of the downstream thermal to magnetic pressure for $\gamma = \frac{5}{3}$. The top and bottom rows correspond to $\beta_1 = 0$ and 2, respectively. The velocity contrast is the ratio, U_{2x}/U_1 , of the normal components of the downstream and upstream flow velocities and is the inverse of the density compression ratio.

The properties of quasi-perpendicular ($\theta_{NB1} > 45^\circ$) and quasi-parallel ($\theta_{NB1} < 45^\circ$) shocks are highlighted by the perpendicular and parallel limiting cases. For quasi-perpendicular shocks, the magnetic compression ratio and velocity contrast are virtually independent of both the shock normal angle and upstream β_1 . They depend primarily on the fast Mach number and approach their strong shock limits by the time M_{f1} reaches 5. The downstream β_2 does depend upon the upstream β_1 , but is still relatively independent of shock normal angle. Perpendicular shocks have the largest magnetic compression ratio and produce the smallest β_2 for a given fast Mach number. However, by the time M_{f1} reaches 3.5, even a perpendicular shock propagating into a cold plasma creates $\beta_2 = 1$ downstream. Thus, if the fast Mach number exceeds 3.5, β_2 is certain to exceed unity.

When $\beta_1 = 0$, all parallel fast shocks with Mach numbers less than 2 switch-on a tangential magnetic field component downstream, and the magnetic compression ratio exceeds unity. When the Mach number exceeds 2, parallel shocks leave the magnetic field unchanged in direction and magnitude. When $C_s^2 > C_A^2$ upstream, there can be no switch-on shock, as in the case $\beta = 2$. The magnetic field never changes, and the shock jump is hydrodynamic in character. Except where switch-on shocks occur, parallel shocks produce a large downstream β_2 , because the magnetic field is not compressed. The magnetic field compression ratio is virtually independent of fast Mach number for quasi-parallel shocks.

The velocity contrast depends significantly on the shock upstream normal angle for $\beta_1 = 0$, whereas it is virtually independent of θ_{NB1} when $\beta_1 = 2$. Since high β_1 shocks are dominated by plasma pressure, their downstream state should depend weakly on the upstream magnetic field magnitude and direction.

Because $\nabla \cdot \mathbf{B} = 0$, the normal component of the mag-

netic field is conserved across plane shocks. However, except for non-switch-on parallel shocks, the tangential component increases. Moreover, the magnetic tension induced by the increased tangential field refracts the downstream flow velocity away from the shock normal. Figure 6 contours the dependences of the angles θ_{NB2} , θ_{NV2} , and θ_{VB2} upon fast Mach number and upstream shock normal angle. \mathbf{N} , \mathbf{B}_2 , and \mathbf{V}_2 are the shock normal, downstream magnetic field, and downstream velocity vectors, respectively. The top and bottom panels are for $\beta_1 = 0$ and 2, respectively. The shaded regions correspond to "subcritical" shocks, discussed in the next section.

The magnetic field does not change direction across perpendicular shocks or across non-switch-on parallel shocks. For all others, the downstream magnetic field is refracted away from the shock normal, as is the velocity. The magnetic field is always more strongly refracted than the flow velocity. When $\beta = 0$, the velocity refraction is especially pronounced for low Mach number, quasi-parallel switch-on shocks. As the Mach number increases, magnetic stresses become proportionally less important, and the change in flow direction across the shock diminishes. When $\beta_1 = 2$, the shock is closer to the gas dynamic limit for which there is no velocity refraction, and the downstream flow velocity makes an angle of 10.8° or less to the shock normal.

In closing, we emphasize that the MHD Rankine-Hugoniot conditions relate the uniform, dissipation-free states of local thermodynamic equilibrium asymptotically far upstream and downstream of the shock. The RH relations are valid only after all the dissipation processes in the spatially nonuniform shock transition have been accounted for. Several such processes are expected to occur and to have different characteristic scale lengths. Of these, the scale length over which the electron and ion temperatures equalize will typically be the longest. In principle, the RH relations apply only to states separated by a distance greater than the longest dissipative scale length.

4. Dissipative MHD Shocks

4.1. Introductory Remarks

A natural first approach to shock structure is to add scalar resistivity, viscosity, and thermal conductivity to the MHD equations and to solve the resulting nonlinear differential equation that describes the transition between the upstream and downstream stationary states. Such an ansatz is almost devoid of physical content, because the plasma processes that lead to dissipation are not specified. Nonetheless, its use has led to one general result—the identification of a critical Mach number above which resistivity cannot provide all the dissipation required by the Rankine-Hugoniot conditions.

Dissipative MHD has a basic scale length for each dissipation process: the lengths that make the magnetic and ordinary Reynolds numbers unity, and a thermal conduc-

MHD RANKINE-HUGONIOT SOLUTIONS

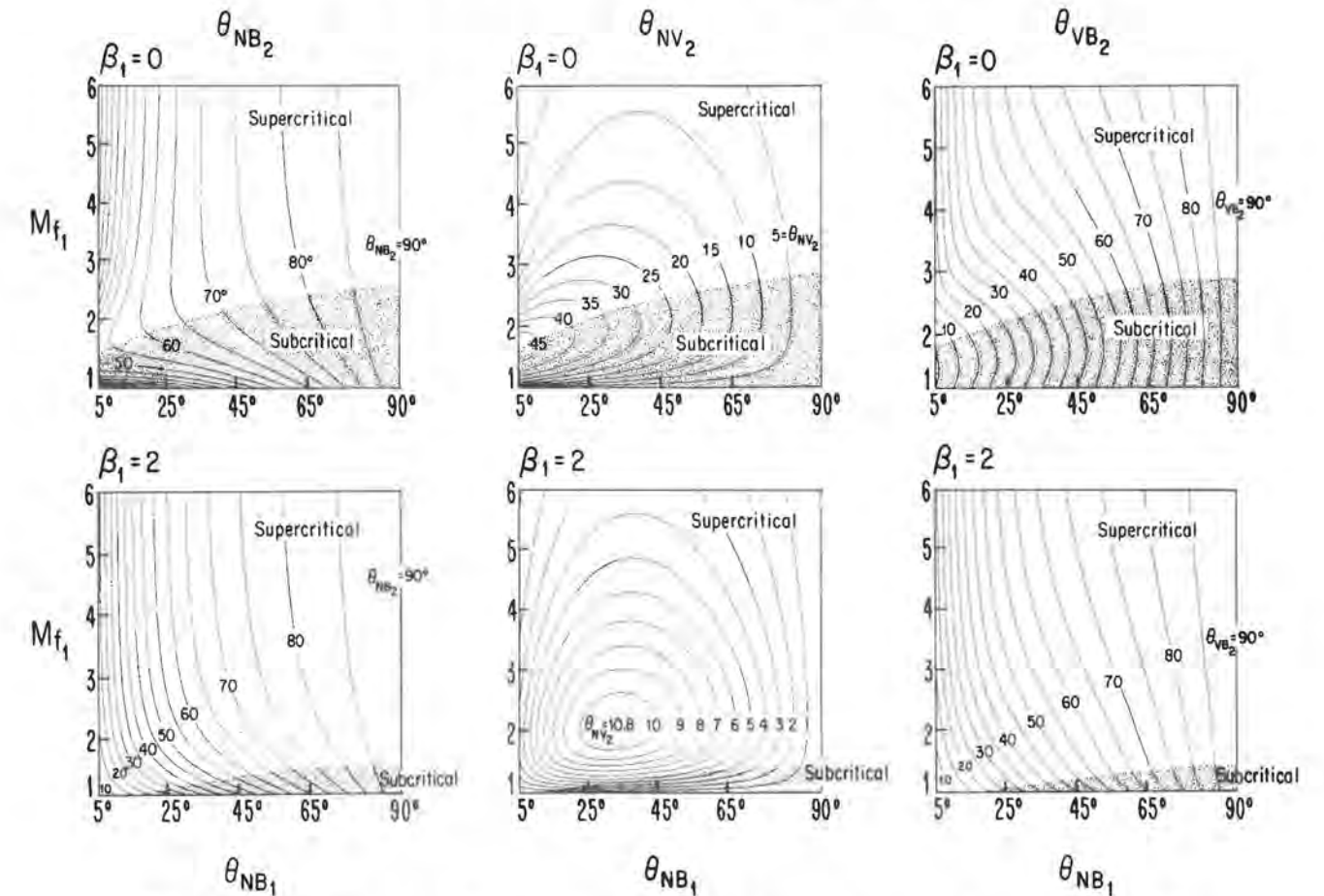


Fig. 6. Fast shock RH relations—downstream angles. Figure 6 contours the dependences of the angles θ_{NB2} between the downstream magnetic field and shock normal, θ_{NV2} , between the shock normal and downstream velocity, and θ_{VB2} , between the downstream velocity and magnetic field, upon the fast Mach number M_{f1} and upstream shock normal angle θ_{NB1} , for $\beta_1 = 0$ (top panels) and $\beta_1 = 2$ (bottom panels).

tion scale length [Coroniti, 1970]. A nonlinear MHD pulse should steepen until it arrives at the longest scale length over which sufficient dissipation occurs to satisfy the Rankine-Hugoniot conditions. The question is, to which length will it steepen? Without a microscopic theory of the dissipation, one cannot go further. Moreover, plasma dissipation is not always a diffusive process, as the fluid description assumes. Nonetheless, the fluid equations do indicate that resistivity can always initiate a fast shock, while viscosity alone cannot provide a complete fast shock transition, and thermal conduction alone is sufficient only for weak shocks [Coroniti, 1970].

The argument above made it natural to investigate when the entire fast shock transition can be accomplished by resistivity. It was always assumed that resistivity would provide enough dissipation for weak shocks. Such shocks would steepen until they arrive at the mag-

netic Reynolds length, and it was up to plasma physics to estimate the anomalous resistivity resulting from the saturation of current-driven instabilities in the shock front, in order to calculate the shock thickness.

The question whether resistivity provides enough dissipation for strong as well as weak shocks was first studied by Marshall [1955]. He found that a perpendicular shock propagating above a fast Mach number of 2.76 into a cold MHD fluid required more dissipation than the maximum possible from resistivity. At the critical Mach number, the normal component of the shock frame downstream flow speed, U_2 , equaled the ordinary sound speed, C_{s2} . It was natural to assume that the additional dissipation was due to viscosity. Indeed within the fluid framework, viscosity was the only option, since finite thermal conductivity cannot provide for strong shocks.

Coroniti [1970] showed that the condition $U_2 = C_{s2}$ de-

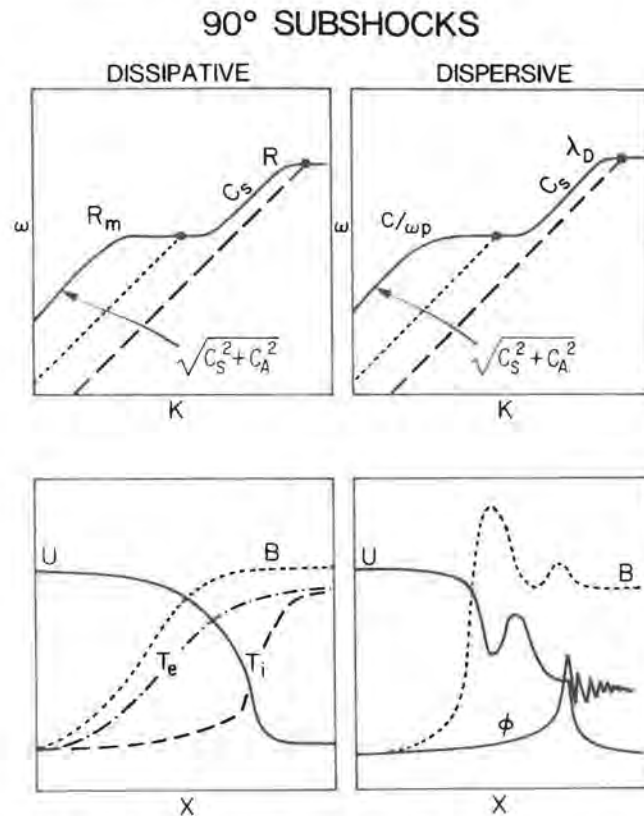


Fig. 7. Ninety degree resistive and dispersive subshocks. The top panels sketch the dispersion relations for a small-amplitude wave propagating perpendicular to the magnetic field in a resistive, viscous, dispersionless plasma (left) and in a dissipation-free, dispersive plasma (right). The shapes of the dispersion curves are similar for both cases. Finite resistivity (left) or finite electron inertia (right) reduces the wave speed from the magnetosonic speed to the sound speed when the wavelength is less than the magnetic Reynolds length (left) or the electron inertial length (right). Finite viscosity (left) or charge separation effects (right) reduce the wave speed to zero when the wavelength is less than the Reynolds length (left) or Debye length (right). The dotted and dashed lines correspond to the flow speeds downstream of subcritical and supercritical shocks respectively. The supercritical shock structures expected in the dissipative and dispersive cases are sketched in the lower left and lower right panels, respectively. The magnetic field increases on the magnetic Reynolds (left) or electron inertial (right) scale lengths, and a viscous (left) or ion sound subshock (right) is embedded within a broader magnetic field structure.

defines a critical Mach number for all upstream parameters, by generalizing an evolutionary argument proposed for the perpendicular fast shock by Kantrowitz and Petschek [1966]. This argument, outlined in section 4.2, considers the conditions for which a downstream fast wave in a resistive MHD fluid can catch the shock. A more formal procedure, which examines the stability of the upstream and downstream stationary states to small perturbations, leads to the same definition of the critical Mach

number. We introduce the stationary point analysis in section 4.3, subsequently add dispersion to resistivity and apply the analysis to dispersive shocks in section 5.2, and finally use it to determine when subcritical shocks should be resistive and when they should be dispersive in section 6.2.

4.2. General Definition of Critical Mach Number

The fast magnetosonic speed in a resistive MHD fluid depends on wavelength, since causality requires that dissipation be accompanied by dispersion:

where

$$\text{Re } C_M^2 = C_S^2 + \text{Re } \bar{C}_A^2 \quad (6)$$

$$\text{Re } \bar{C}_A^2 \approx \frac{C_A^2}{1 + k^2 R_m^2} \quad (7)$$

and R_m is the magnetic Reynolds length,

$$R_m = \frac{c^2}{4\pi\sigma V_{ph}} \quad (8)$$

c is the speed of light, σ the electrical conductivity, V_{ph} the phase speed, and k the wave number. Re , here, denotes the real part of the expression following it.

The dispersion relation for a perpendicular fast wave in a resistive and viscous fluid is sketched in the upper left-hand panel of Figure 7. The dotted and dashed lines correspond to the fluid velocity downstream of a subcritical and supercritical shock, respectively. The phase speed approaches the magnetosonic speed of ideal MHD in the long-wavelength limit. Finite resistivity progressively decouples the magnetic and fluid oscillations as the wavelength decreases, so that the phase speed ultimately approaches the sound speed, C_S , when the wavelength is comparable to the magnetic Reynolds length. By adding the dispersion due to viscosity, presumed to set in at a shorter Reynolds length, R , Coroniti [1970] showed that the phase speed finally approaches zero when $kR \gg 1$.

Imagine that a piston launches a nonlinear magnetosonic pulse which steepens into a shock whose scale length is the magnetic Reynolds length. The piston now launches another magnetosonic wave which, by the evolutionary conditions, must overtake the shock. This wave also steepens until it arrives at the magnetic Reynolds length and its propagation speed is reduced to the sound speed. If $U_2 > C_{S2}$, it cannot reach the shock, and the shock is steady. If, however, $U_2 < C_{S2}$, the wave overtakes the shock, causing it to steepen until the next smaller dissipation length is reached. Since viscosity reduces the wave speed to zero, viscosity can always provide whatever dissipation is needed for supercritical shocks.

The supercritical shock structure expected from the above arguments is sketched in the lower left-hand panel of Figure 7. The magnetic field and the temperature of the electrons, which are resistively heated, should in-

FIRST CRITICAL MACH NUMBER $M_{f_1}^*$

$$u_{2x} = c_{s2} \quad (\gamma = 5/3)$$

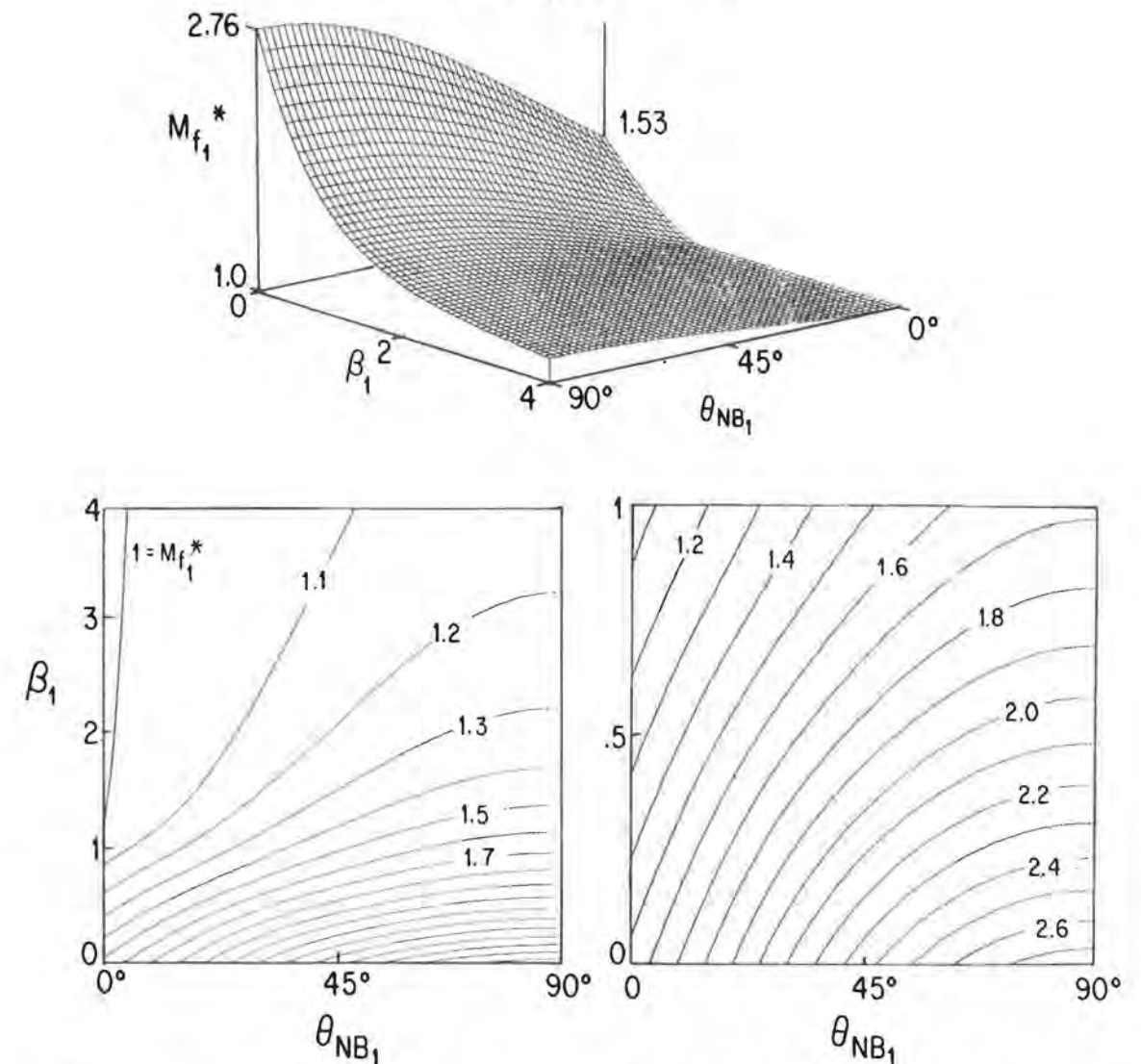


Fig. 8. Parameter dependence of the critical Mach number. The critical Mach number is defined as that for which the normal component of the downstream flow speed in the shock frame, U_{2x} , equals the sound speed C_{S2} . The top panel shows the dependence of the critical Mach number on the upstream thermal β_1 and shock normal angle θ_{NB1} for $\gamma = \frac{5}{3}$. The lower panels contour the same dependences for $0 < \beta_1 < 4$ (left) and for $0 < \beta_1 < 2$ (right). The critical Mach number is a strong function of upstream plasma parameters. When $\beta_1 = 0$, it decreases from 2.76 at $\theta_{NB1} = 90^\circ$ to 1.53 when $\theta_{NB1} = 0^\circ$. When $\beta_1 > 1$, it is close to unity for all upstream shock normal angles.

crease smoothly on the resistive scale length, whereas the temperature of the ions, which are heated by viscosity, should increase across a thin embedded subshock whose scale length is the Reynolds length. Part of the density increase and the associated decrease in fluid ve-

locity should take place on the resistive scale length, and part in the viscous subshock.

The above argument can be extended from perpendicular to oblique fast shocks by noting that in resistive MHD, the speed \bar{C}_A always replaces the Alfvén speed in

the fast mode dispersion relation, so that when $kR_m > 1$, all fast modes propagate at the sound speed. Thus, equating the normal component of the downstream flow velocity to the downstream sound speed defines, for all shock normal angles and all upstream conditions, a critical Mach number above which resistivity is unable to provide all the required shock dissipation.

4.3. Stationary Point Analysis

To solve for the full shock structure, the dissipative MHD equations should be reduced to a nonlinear differential equation that describes the change in one of the fluid variables between the upstream and downstream stationary points. The fluid variables at the two stationary points satisfy the RH relations. Some of the effects of dissipation on shock structure can be obtained by studying the linear development of small perturbations at the stationary points [Coroniti, 1970]. For a proper shock transition, dissipation must cause an upstream perturbation to increase approaching the shock, and all downstream perturbations to die away leaving the shock.

After equating the coefficients of viscosity and thermal conductivity to zero, and perturbing fluid variables about the upstream or downstream stationary points, we arrive at the following differential equation which describes the evolution in the shock frame of the tangential magnetic field [Coroniti, 1970]:

$$R_m \delta B_z' = D(U) \delta B_z = \frac{(U^2 - C_F^2)(U^2 - C_{SL}^2)}{U^2(U^2 - C_S^2)} \delta B_z \quad (9)$$

where superscript prime denotes an x derivative, $R_m = c^2/4\pi\sigma U$ is the magnetic Reynolds length, and σ is the electrical conductivity. Note that the definition of R_m used in (9) differs slightly from (8). We chose a Cartesian coordinate system such that the shock normal is parallel to the negative x axis, and the magnetic field upstream and downstream is contained in the x - z plane.

Equation (9) applies to all shocks, and to both their upstream and downstream states. The Rankine-Hugoniot conditions must be used to determine the magnetic field direction, the flow speed, and the fast, slow, and sound speeds in the downstream state. For the argument to follow, we will need only the most general properties of the RH solutions. Since $U^2 > C_F^2 > C_S^2 > C_{SL}^2$ upstream of fast shocks, the quantity D is positive upstream, and (9) indicates that resistivity initiates the shock by causing δB_z to grow approaching the shock. The Rankine-Hugoniot conditions require that $C_F^2 > U^2 > C_{SL}^2$ downstream, so that the sign of D changes when the downstream flow speed equals the sound speed. When $U^2 > C_S^2$ downstream, resistivity damps all magnetic perturbations with increasing distance downstream of the shock. On the other hand, when $U^2 < C_S^2$, δB_z grows downstream, and the purely resistive shock is unstable. An additional dissipation mechanism is therefore required to complete the shock transition. This stationary point analysis confirms the conclusion drawn from evolutionary arguments.

4.4. Parametric Dependence of Critical Mach Number

The dependence of the fast critical Mach number M_{F1}^* on the upstream shock normal angle θ_{NB1} and plasma β_1 is shown in Figure 8 [Edmiston and Kennel, 1984]. Marshall's [1955] original result, $M_{F1}^* = 2.76$, occurs only for $\theta_{NB1} = 90^\circ$ and $\beta_1 = 0$. The critical Mach number for a perpendicular shock decreases to slightly above unity when $\beta_1 > 1$. For a parallel shock propagating into a cold plasma it is 1.53, and it, too, decreases as β_1 increases. It is exactly unity whenever C_S^2 exceeds C_A^2 upstream and $\theta_{NB1} = 0^\circ$.

Note that the critical Mach number is less than 2 for typical solar wind parameters, rather than the often quoted value of 2.76. This fact, which is not widely appreciated, implies that nearly all bow shocks are supercritical.

4.5. Summary

1. Equating the normal component of the downstream shock frame flow speed to the sound speed defines a critical fast Mach number above which resistivity alone cannot provide all the dissipation required by the shock jump conditions.

2. The critical Mach number is a strong function of the upstream thermal β_1 and shock normal angle. For typical solar wind parameters, it is less than 2.

3. Another dissipation mechanism in addition to resistivity must play a role in supercritical shocks. Although in MHD it is natural to assume that viscosity is the second dissipation mechanism, anything that converts flow momentum into heat will do.

In closing, we note that the critical Mach number is defined by a limiting argument that indicates when a second dissipation mechanism must exist. It need not suddenly turn on at the critical Mach number, and it could well be present in subcritical shocks.

5. Dispersive Shocks

5.1. Introductory Remarks

The two-fluid model of plasmas contains three basic scale lengths, the electron and ion inertial scale lengths, c/ω_{pe} and c/ω_{pi} , respectively, and the Debye length, λ_D , which represent the facts that changes in electron or ion currents and in charge density cannot take place instantaneously. The small-amplitude waves described by two-fluid theory are therefore dispersive, although they approach nondispersive MHD waves in the long-wavelength limit [Stringer, 1963; Formisano and Kennel, 1969]. In this section, we discuss the shock structure expected in those cases where a nonlinear pulse steepens to dispersive scale lengths before it arrives at the resistive scale length defined in section 4.

Dispersion can limit wave steepening. As a compressional wave steepens, flow nonlinearities populate the short-wavelength dispersive part of its Fourier decomposition spectrum. The short-wavelength energy is carried away by a nonlinear wave radiated by the steepening

front. Dissipation, always necessary, ultimately damps the nonlinear wave, and a steady, spatially oscillatory shock is formed.

Many properties of nonlinear dispersive wave trains can be inferred from those of the corresponding linear waves. Whether the short-wavelength linear waves propagate faster or slower than the MHD fast speed determines whether the wave train leads or trails the main shock ramp. The nonlinear wave train must damp to a small-amplitude wave asymptotically far from the shock. Since the entire wave train is time stationary in the shock frame, the asymptotic small-amplitude wave must phase stand in the flow. Thus, the oscillatory scale length of the wave train may be estimated from the wavelength of the corresponding small-amplitude wave that phase stands in the far upstream or far downstream flow. Furthermore, since the dispersive wave must carry energy away from the steepening shock front, its small-amplitude group velocity should be greater than the upstream flow speed, if it stands upstream. Similarly, its group velocity should be less than the downstream flow speed, if it stands downstream.

We begin by considering perpendicular dispersive shocks in section 5.2. Once again, the dispersion relation of small-amplitude waves suggests the existence of a critical shock transition when the downstream flow speed equals the sound speed. This suggestion is confirmed by a generalization of the stationary point analysis of section 4.3 to include both finite electron inertia dispersion and resistivity. A resistively damped wave train with a c/ω_{pe} scale length stands downstream of subcritical shocks, whereas new forms of dispersion and dissipation are required for supercritical shocks.

Finite ion inertia plays no role in exactly perpendicular shocks, but it dominates the dispersive structure of even slightly oblique small-amplitude waves and shocks [Galeev and Karpman, 1963; Karpman, 1964]. In section 5.3, we infer the properties of oblique nonlinear wave trains from the dispersion relation of the corresponding small-amplitude waves. We will calculate the maximum Mach number for which a nonlinear dispersive whistler can stand upstream, and comment upon the possible structure of supercritical oblique shocks.

5.2. 90° Dispersive Shocks

The two-fluid magnetosonic wave dispersion relation in the quasi-neutral approximation is formally similar to (6):

$$\omega^2/k^2 = C_S^2 + \frac{C_A^2}{1 + k^2 R_e^2} = C_S^2 + \bar{C}_A^2 \quad (10)$$

where R_e is the electron inertial length c/ω_{pe} . We have neglected dissipation so that $R_m \ll R_e$ [Formisano and Kennel, 1969]. As kR_e increases, finite electron inertia progressively decouples the magnetic field from the fluid oscillations, and the phase speed decreases from the magnetosonic speed to the sound speed. Since the phase speed decreases, the nonlinear wave train will trail the

shock. Since its group speed is less than its phase speed, it will carry energy away from the shock. Such a wave can stand downstream only of subcritical shocks, since its phase velocity always exceeds the sound speed.

The generalization to a two-fluid quasi-neutral plasma of the stationary point differential equation for a perpendicular shock is

$$R_e^2 \delta B_z'' + R_m \delta B_z' = D \delta B_z = \frac{U^2 - C_M^2}{U^2 - C_S^2} \delta B_z \quad (11)$$

when ion pressure and finite ion Larmor radius effects are neglected [Coroniti, 1971]. Assuming solutions of the form $\delta B_z \sim e^{\lambda x}$, we find

$$\lambda_{\pm R_e} = \frac{-R_m \pm (R_m^2 + 4R_e^2 D)^{1/2}}{2R_e} \quad (12)$$

Since $D(U_1) > 0$ upstream, there exists one solution, λ_+ , for which δB_z grows exponentially approaching the shock, and one, λ_- , which violates the boundary condition that $\delta B_z \rightarrow 0$ far upstream of the shock. It is easy to show that the scale length $\Delta = 1/\lambda_+$ of the leading edge of the shock is approximately

$$\Delta \approx R_e/D^{1/2}(U_1) \quad (13)$$

when $R_m \ll R_e$, and

$$\Delta \approx R_m/D(U_1) \quad (14)$$

when $R_e \ll R_m$. Thus, the shock thickness scales as the larger of the magnetic Reynolds length and the electron inertial length, the conclusion expected from steepening arguments.

$D(U_2)$ is negative downstream of subcritical shocks. Therefore, the downstream asymptotic solution is an oscillatory wave train which is weakly damped by resistivity if $R_m \ll R_e$. It can be shown, using (11) and (13), that its wave number satisfies the phase-standing condition. On the other hand, since $D(U_2)$ is positive downstream of supercritical shocks, the λ_+ solution grows with distance downstream, indicating that steepening will continue until new forms of dissipation or dispersion complete the shock transition.

The quasi-neutral approximation used in (10) and (11) breaks down when the supercritical shock steepens to the Debye length. When the dispersive effects at the electron inertial length and the Debye length are both included, the two-fluid dispersion relation for small-amplitude magnetosonic waves has a form similar to that in a resistive-viscous fluid, as may be seen by comparing the upper left-hand and right-hand panels of Figure 7. The dotted line in the upper right-hand panel corresponds to the flow speed downstream of a subcritical dispersive shock, in which a trailing wave with a c/ω_{pe} scale length stands. The dashed line in the upper right-hand panel corresponds to the flow speed downstream of a supercritical dispersive shock. Since Debye length dispersion reduces the phase speed, a trailing electrostatic ion sound wave with a Debye length scale will stand down-

stream. Since the plasma currents cannot follow oscillations with scales less than the electron inertial length, the electrostatic oscillations will be decoupled from those of the magnetic field, and the nonlinear ion sound wave train will form a subshock that is embedded in a broader magnetic field structure. This wave train is expected to be similar to the one that forms in an unmagnetized plasma [Sagdeev, 1979]. Another form of dissipation, besides resistivity, is required to damp the ion sound wave train and complete the supercritical shock transition.

The variations in flow parameters across a supercritical dispersive shock are sketched in the bottom right-hand panel of Figure 7. The magnetic field forms a trailing wave train with an electron inertial scale length. The number of magnetic field oscillations depends upon the resistive damping rate. Embedded in the magnetic field structure near the local sonic point is a dispersive ion sound subshock, illustrated by the Debye length oscillations (not to scale) in the electrostatic potential ϕ . Part of the reduction in flow speed required by the RH relations occurs across the electron inertia wave train, and part across the ion sound subshock.

At this point, we approach the limits of fluid theory. Nonlinear ion sound waves are damped, and rendered irreversible, by ion reflection, a nonfluid effect [Moiseev and Sagdeev, 1963; Sagdeev, 1979]. This indicates that the extra dissipation needed for supercritical shocks cannot be anything as simple as viscosity. Nonetheless, the two-fluid equations have served us well, for they too indicate the existence of the supercritical shock transition and, also, some of the physics needed to describe supercritical shocks.

5.3. Oblique Dispersive Shocks

The left-hand panel of Plate 1 sketches the quasi-neutral two-fluid dispersion relation for C_S^2/C_A^2 small and oblique propagation [Formisano and Kennel, 1969]. It has three branches whose phase speeds approach the three MHD speeds in the long-wavelength limit. At shorter wavelengths, the fast mode is converted into an elliptically polarized whistler wave whose speed exceeds the fast MHD speed. Finite ion inertia progressively decouples the ion mass from the magnetic field oscillations as the wavelength of the fast mode decreases. Its phase speed therefore increases and approaches a maximum of about the electron Alfvén speed, in which only the electron mass inertially loads the magnetic field oscillations. Finite electron inertia then begins to decouple the magnetic field and fluid oscillations, and its phase speed decreases. Eventually, it approaches the sound speed, at which point the fast mode is entirely electrostatic. The intermediate speed decreases to the sound speed, and the slow speed tends to zero, as the wavelength decreases.

The right-hand panel of Plate 1 sketches the two-fluid quasi-neutral dispersion relation for oblique propagation and $C_S^2/C_A^2 > 1$. There are two important differences with respect to the previous $C_S^2/C_A^2 < 1$ case. First, the

wavelength at which the whistler phase speed first exceeds the fast speed and the ratio of the maximum whistler phase speed to the fast speed both decrease with increasing C_S^2/C_A^2 . Second, when $C_I = C_A \cos \theta < C_S$, the intermediate speed increases to the sound speed at ion inertial wavelengths.

The fact that the fast wave speed increases with decreasing wavelength implies that the nonlinear wave train will lead oblique shocks, in contrast to the 90° case discussed above. We may use an evolutionary argument to determine the shock normal angle at which the wave train switches from trailing to leading. The upstream ion inertial scale length, R_i , is determined rigorously in Coroniti's [1971] derivation of the stationary point differential equation (22)–(24) described in the next section:

$$R_i = \frac{c}{\omega_{pi}} \frac{C_I}{U_1} = \frac{c}{\omega_{pi}} \frac{C_A \cos \theta_{NB1}}{MC_F} \quad (15)$$

Note that R_i tends to zero as θ_{NB1} approaches 90° . The ion inertial scale length for small-amplitude waves may be obtained by setting the fast Mach number, M , equal to unity in (15). A nonlinear pulse will steepen until it encounters the first scale length at which a dispersive shock can form. Thus, if $R_i > R_e$, the wave train will lead the shock, and vice versa. Equating R_i to R_e defines the shock normal angle θ_{NB1}^* at which the dispersive structure changes:

$$\cos \theta_{NB1}^* = \left(\frac{M_e}{M_i} \right)^{1/2} \frac{MC_F}{C_A} \quad (16)$$

where m_e and M_i are the electron and ion mass, respectively. For a low β_1 hydrogen plasma and $M \approx 1$, the angle θ_{NB1}^* is approximately 87° . Thus, we expect leading ion inertial wave trains for nearly all shock normal angles. The trailing 90° electron inertial wave train has never been definitively identified in space.

Let us now calculate the upper limit fast Mach number for which a whistler can phase-stand in the upstream flow. The dash-dotted lines in either panel of Plate 1 indicate that the upstream flow speed intersects the fast mode branch provided that it is below the maximum whistler phase speed. The top and bottom panels of Figure 9 show, in polar and contour formats, respectively, the dependence on shock normal angle and upstream C_S^2/C_A^2 of the fast Mach number corresponding to the maximum whistler phase speed. No wave train stands ahead of perpendicular shocks, and the "whistler critical Mach number," which is relatively small for very oblique shocks, increases rapidly with decreasing θ_{NB1} and approaches an upper limit of $\frac{1}{2}(M_i/m_e)^{1/2} \approx 22$ for parallel shocks in zero β_1 hydrogen plasmas. The whistler critical Mach number at all θ_{NB1} decreases rapidly once C_S^2 exceeds C_A^2 upstream. Above the whistler critical Mach number, the shock will be initiated by a monotonic ramp on electron inertial scales when $R_m \ll R_e$. It is particularly important to note that for typical solar wind param-

eters an upstream whistler wave train need not form if the shock is sufficiently oblique and has a sufficiently high Mach number.

We next consider the waves that phase-stand downstream of shocks, focusing on the subcritical case first.

The dashed lines in Plate 1 indicate a flow speed between the fast and intermediate speeds, the state downstream of fast shocks. The left-hand panel, applied to the downstream state, corresponds to a subcritical shock with $U_2 < C_{S2}$. In this case, a short-wavelength whistler standing in the downstream flow can carry energy away from the shock, thereby leading to a stable shock transition when the downstream whistler is damped by resistivity.

The right-hand panel, which, when it is applied to the downstream state, corresponds to a supercritical shock, suggests that a dispersive mode on the intermediate branch could stand downstream. Because its group velocity exceeds the downstream flow speed, it could carry energy towards the shock and therefore might cause the shock to steepen. However, since the long-wavelength MHD intermediate wave does not steepen, evolutionary arguments shed no light on how such a standing wave might develop. Debye length dispersion is also expected at short wavelengths. In short, although it has not been investigated in detail, a definite change in the structure of oblique dispersive shocks at the critical Mach number is predicted by two-fluid theory.

5.4. Summary

We have outlined the physical picture of shock structure that emerges from two-fluid theory. The two-fluid approximation contains ion and electron inertial scale lengths in the quasi-neutral approximation, and, in addition, the Debye length, when quasi-neutrality is relaxed. Small-amplitude waves are dispersive at each of these basic scale lengths. When the ion β is significant, low-frequency waves are also dispersive at ion cyclotron wavelengths [Fredericks and Kennel, 1968; Coroniti, 1971], an effect we neglected in order to focus on the classical wave train analyses in the literature. Our discussion is therefore strictly valid for plasmas in which the ratio of electron to ion temperature is large, though we believe it illuminates shock behavior over a wider range of plasma parameters.

We tacitly assumed that all dissipative scale lengths are shorter than all pertinent dispersive scale lengths in order to emphasize the possible dispersive wave trains expected from two-fluid theory. We reached the following conclusions:

1. Finite electron inertia dispersion creates a trailing wave train with a c/ω_{pe} magnetic field scale length downstream of perpendicular subcritical shocks.
2. Supercritical magnetosonic shocks steepen to form a trailing ion sound dispersive subshock. The dissipation required to damp the ion sound wave train and thereby complete the shock transition cannot be resistivity.
3. Finite ion inertia dispersion creates a leading whistler wave train with the scale length R_i (defined in (15)) upstream of oblique shocks. Leading ion inertial wave trains are expected for nearly all shock normal angles.
4. Above the whistler critical Mach number defined in section 5.3, a small-amplitude whistler cannot stand in

MAXIMUM FAST MACH NUMBER FOR LEADING WHISTLER WAVETRAINS

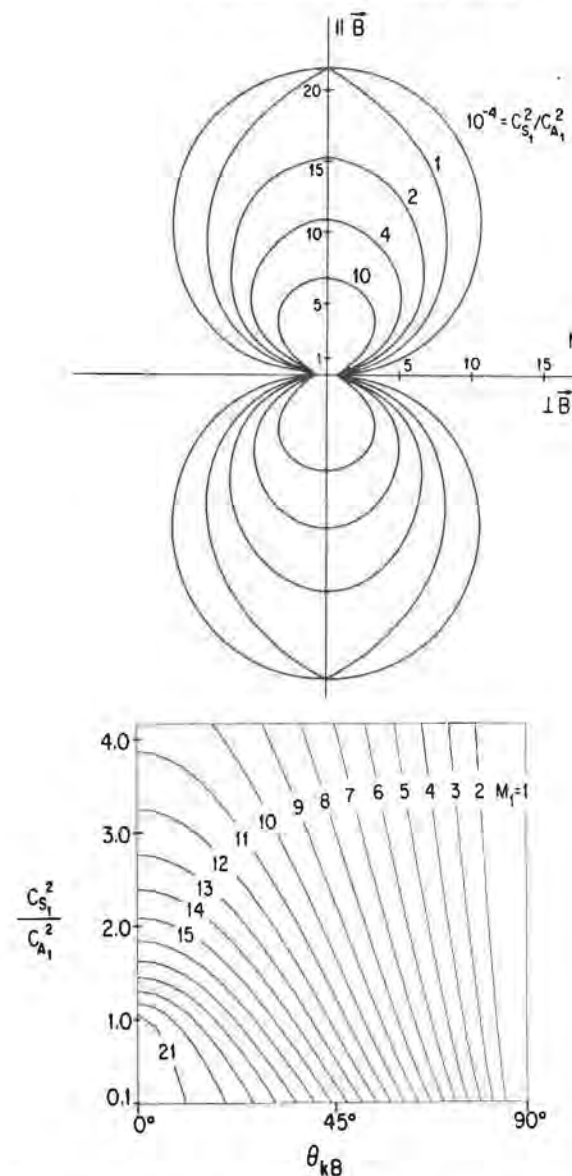


Fig. 9. Whistler critical Mach number. The top and bottom panels show the dependence on shock normal angle and upstream C_S^2/C_A^2 of the fast Mach number above which a whistler wave cannot stand in the upstream flow, in polar and contour formats, respectively. The radial coordinate in the polar diagram is the fast Mach number, and the angular coordinate is the shock normal angle.

the upstream flow, and the shock will be initiated by a monotonic ramp with a c/ω_{pe} scale length.

5. Inspection of the two-fluid dispersion relation suggests that supercritical oblique shocks potentially involve downstream oscillations on the intermediate branch. An electrostatic ion sound wave train may also form.

This section primarily illustrated the content of classical theoretical structures obtained in the weak dissipation limit, and not necessarily the true structure of shocks. To approach greater realism, it is necessary to specify the shock dissipation mechanisms and to grapple with the limitations of the fluid approach.

1. A microscopic theory of resistivity is needed to decide whether subcritical shocks will be resistive or dispersive (section 6).

2. The weak dissipation limit probably does not apply to supercritical shocks, although it does define the critical shock transition. It is dangerous to proceed above the critical Mach number without including the new dissipation processes that must operate. For example, without explicitly considering the dissipation, one cannot say for sure whether nonlinear whistlers will stand upstream of supercritical shocks.

3. The use of fluid theory requires that heat flow parallel to the magnetic field be neglected, an assumption which is suspect for quasi-parallel shocks.

6. Subcritical Shocks With Ion Sound Anomalous Resistance

6.1. Introductory Remarks

Sections 4 and 5 summarized two very different theories of subcritical shock structure, one of which predicts a monotonic shock jump and the other an oscillatory wave train. Both types have been found in studies of the earth's bow shock. According to the thickest shock hypothesis, nonlinear steepening is limited by dissipation or dispersion, whichever occurs first. Since resistivity is the only dissipation required for subcritical shocks we need only compare the resistive and dispersive scale lengths to decide whether a subcritical shock will be resistive or dispersive. This can only be done by examining the theory of anomalous resistivity in collisionless plasmas.

6.2. Ion Sound Anomalous Resistance

Since the earliest investigations of collisionless shocks [Sagdeev, 1966], it has been believed that the ion sound instability could provide the anomalous resistivity necessary to complete the subcritical shock transition. The theoretical reasons for this belief have been good ones. The ion sound instability has a low current threshold when the electron temperature exceeds the ion temperature. It produces Debye length electrostatic fluctuations which are microscopic compared to the electron inertial length, so that fluid theory may be used even for perpendicular shocks. When the electron plasma frequency ex-

ceeds the electron cyclotron frequency, as it does in the solar wind, ion sound waves are essentially unmagnetized and can interact with the bulk of the electron distribution, so that runaway can be prevented for most of the electrons. Finally, since resistivity implies the transfer of momentum from streaming electrons to ions, a good anomalous resistivity instability must involve both electrons and ions, as the ion sound instability does.

The quasi-linear theory of the ion sound instability is well understood [Galeev, 1976]. When $T_e \gg T_i$, its growth rate, γ , is

$$\gamma = (M_e/M_i)^{1/2} (\omega/kC_s)^{-3} [\mathbf{k} \cdot \mathbf{V}_{De} - \omega] \quad (17)$$

where $C_s = (T_e/M_i)^{1/2}$, the ion sound speed, ω and \mathbf{k} are the frequency and wave vector, respectively, and \mathbf{V}_{De} is the electron drift velocity associated with the current. Since ion sound waves obey

$$\omega^2 = \frac{k^2 C_s^2}{1 + k^2 \lambda_D^2} \quad (18)$$

where λ_D is the electron Debye length, they will be unstable when $V_{De} > C_s$.

In steady state anomalous resistance, the waves radiated by drifting electrons must be absorbed by ions, in order that electron momentum be transferred to ions. The ion distribution therefore develops a high-energy tail extending to speeds comparable to the ion sound speed. The electron distribution develops a flat top at low velocities [Sagdeev and Galeev, 1969; Dum, 1978a, b]. A self-similar solution with the following properties has been found [Bekshstein and Sagdeev, 1970; Bekshstein et al., 1971; Dum, 1978a, b]

$$\begin{aligned} V_{De}^* &= C_s (M_i/M_e)^{1/4} \\ T_{Hi} &= T_e \quad X = (M_e/M_i)^{1/4} \end{aligned} \quad (19)$$

where T_{Hi} is the effective temperature and X the fractional density of the hot ion tail. V_{De}^* , above, is the speed at which the electron drift is limited by ion sound anomalous resistance.

The above quasi-linear solution, the one most pertinent to typical solar wind conditions, is valid for relatively small driving currents and electric fields. For stronger driving fields, the bulk of the ion distribution is heated by nonlinear Landau damping, and the limiting V_{De} increases. When $T_e \approx T_i$, V_{De} must be comparable with the electron thermal speed for unstable growth, and the ion sound instability passes to the so-called Buneman [1959] limit. Galeev [1976] discusses these strongly driven regimes of the ion sound instability, a relatively academic topic insofar as most collisionless shocks in space are concerned.

6.3. Resistive Dispersive Transition

We may estimate the anomalous magnetic Reynolds length, R_m^* , as follows. For the shock geometry used in

RESISTIVE-DISPERSIVE TRANSITION FOR SUBCRITICAL FAST SHOCKS

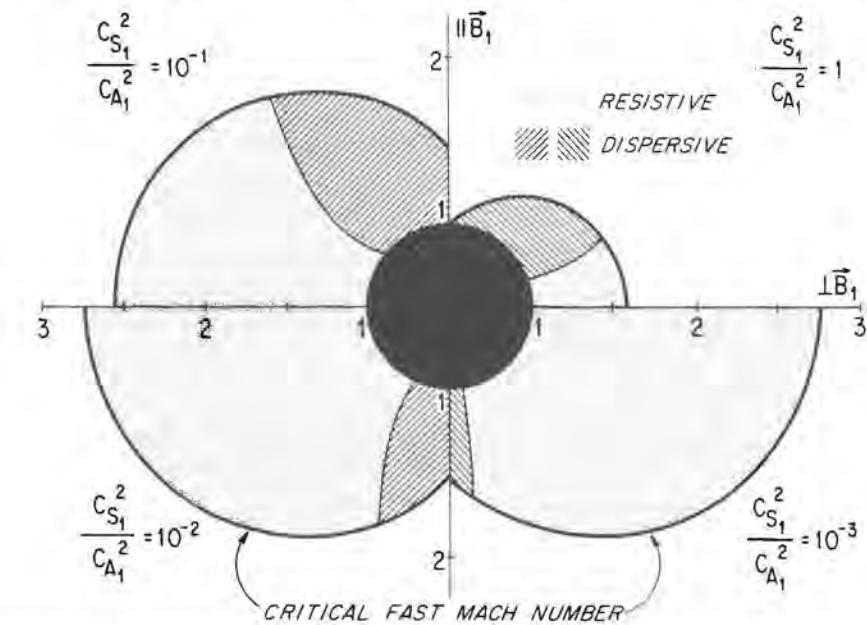


Fig. 10. Subcritical resistive-dispersive transition. Each quadrant is a different Friedrichs diagram for $C_s^2/C_A^2 = 10^{-3}, 10^{-2}, 10^{-1}$, and 1 upstream in which the radial coordinate is the fast Mach number and the angular coordinate is the shock normal angle. The critical Mach number is indicated by the thick solid curves bounding each diagram. Subcritical shocks should be resistive in the shaded regions, and dispersive in the hatched regions.

(6) and (11), Ohm's law reduces to

$$j_y = \sigma \left(E + \frac{U \times B}{c} \right)_y \approx \sigma \frac{U_1 B_{z1}}{c} \quad (20)$$

Assuming that $\sigma^* U_1 B_{z1}/c \approx ne V_{De}^*$, we find, using (19),

$$R_m^* = \frac{c^2}{4\pi\sigma^* U_1} \approx \frac{c}{\omega_{pi}} (M_e/M_i)^{1/4} \beta_e^{-1/2} \sin \theta_{NB1} \quad (21)$$

$\beta_e = 8\pi n T_e/B^2$. The estimate (21) is probably accurate up to a numerical factor of order unity [Galeev, 1976].

We estimate the parameter dependence of the resistive-dispersive transition by substituting R_m^* , calculated using upstream parameter values, into the upstream stationary point differential equation that takes finite electron and ion inertia and resistivity into account, assuming quasi-neutrality [Coroniti, 1971]:

$$R_e^2 \delta B_z'' + R_m^* \delta B_z' - R_i \delta B_z' = D(U_1) \delta B_z \quad (22)$$

$$R_e^2 \delta B_y'' + R_m^* \delta B_y' + R_i \delta B_z' = (1 - C_1^2/U_1^2) \delta B_y \quad (23)$$

where the upstream ion inertial scale length R_i is

$$R_i = (c/\omega_{pi}) C_1/U_1 \quad (24)$$

when the ion pressure may be neglected. Since upstream whistlers are elliptically polarized, the z and y components of the magnetic field perturbation are coupled in (22)–(24).

Choosing an e^{ix} spatial dependence reduces (22)–(24) to a quartic, one of whose four solutions corresponds to an upstream whistler that is resistively damped as it propagates away from the shock. We then seek the conditions for which $\text{Re } \lambda = \text{Im } \lambda$. The whistler radiated by the steepening shock would then be damped after it propagates one wavelength upstream, and the shock transition would be monotonic. Our procedure is therefore based on the assumption that the nonlinear scale length and the wavelength of the upstream phase-standing wave are comparable. Its formal results are not valid above the critical Mach number, because the additional dissipation needed has not been taken into account in calculating the whistler damping length.

Figure 10 shows the curve $\text{Im } \lambda = \text{Re } \lambda$ in a polar plot whose radial coordinate is the fast Mach number and whose polar angle is the shock normal angle. The critical Mach number is also shown. Each quadrant corresponds to a different value of C_s^2/C_A^2 upstream. We assumed that $T_e/T_i \gg 1$. In general, quasi-parallel shocks should be dispersive and quasi-perpendicular shocks resistive. The range of θ_{NB1} for which the shock is resistive increases with increasing Mach number, and for a given Mach number, the resistive θ_{NB1} range decreases with increasing C_s^2/C_A^2 upstream.

Mellott and Greenstadt [1984] have summarized the existing data on the resistive-dispersive transition in sub-

critical bow shocks. They calculated the resistive and dispersive scale lengths using *Galeev's* [1976] estimates of ion sound anomalous resistance and measured values of the density, θ_{NB1} , and β_{e1} . They found that for shocks with upstream wave trains, the dispersive scale length exceeded the ion sound resistive scale length, whereas, with one exception, monotonic shocks corresponded to the opposite limit.

6.4. Summary

1. When Te/Ti is large, the ion sound instability has a low current threshold.
2. When $\omega_{pe}/\Omega_{ce} \gg 1$, as it is in the solar wind, ion sound anomalous resistance limits V_{De}^* to $(M_i/M_e)^{1/4} C_S$ in the quasi-linear regime. The corresponding Reynolds length, R_m^* , is approximately

$$R_m^* \approx c/\omega_{pi} (M_e/M_i)^{1/4} \beta_e^{-1/2} \sin \theta_{NB1}$$

3. When R_m^* exceeds the dispersive scale length, a subcritical shock will be resistive, and dispersive otherwise. A slightly more sophisticated criterion for the resistive-dispersive transition was developed in section 6.2.
4. When the electron β_e is very small, nearly all subcritical shocks are resistive. For the range of β_e appropriate to most solar wind shocks, the more perpendicular subcritical shocks will be resistive, and the more parallel shocks will be dispersive.
5. Observations of subcritical bow shocks appear to agree with the ion sound theory of the resistive-dispersive transition.

The relatively complete treatment of ion sound anomalous resistance remains the prototype for theories of other microinstabilities in collisionless shocks. The illustrative computations presented here are strictly valid only for large Te/Ti and small upstream β_1 . As β_1 increases, it becomes increasingly difficult for magnetic gradients to induce an electron drift speed that exceeds the ion sound speed. The ion sound critical drift also increases as Te/Ti decreases. In fact, Te/Ti is often so small in the solar wind that theoreticians sometimes question whether the ion sound instability should occur. (This makes *Mellott and Greenstadt's* [1984] result somewhat puzzling.) When Te/Ti is small, other current instabilities, such as the modified two-stream or the lower hybrid drift instabilities [*Lemons and Gary, 1978; Winske, this volume*] may be important. Because the ion inertial scale length increases with decreasing θ_{NB1} , quasi-parallel subcritical shocks will continue to be dispersive, and quasi-perpendicular shocks resistive, when other instabilities provide the anomalous resistance. The quantitative specification of the resistive-dispersive transition will, of course, differ. Finally, there may even exist conditions for which anomalous resistance may not develop at all, for example, in high β quasi-parallel shocks.

7. Supercritical Quasi-Perpendicular Shocks

7.1. Introductory Remarks

Nearly all bow shocks are supercritical. Nearly all quasi-perpendicular bow shock magnetic field profiles resemble the one in the top panel of Figure 11, rather than the resistive or dispersive profiles predicted by fluid theory. They consist of a foot, a ramp, and at least one overshoot-undershoot cycle downstream. Instead of a leading whistler wave train with an ion inertial scale length, the overshoot-undershoot resembles a trailing wave train whose scale length is an ion Larmor radius.

Classical fluid theory had suggested the new physics required beyond the supercritical transition. Ions would reflect from the Debye length electrostatic potential layer that would develop above the critical Mach number. If the upstream magnetic field were weak, reflected ions would free stream away from the shock. Ion-ion instabilities induced by the relative streaming of incoming and reflected ions would produce a turbulent viscosity which would decelerate the incoming flow and regulate the size of the potential jump. Many early experiments [*Paul et al., 1965, 1967; Keilhacker et al., 1972; Segre and Martone, 1971*] and simulations were effectively in the weak field regime, because they were completed in less than one upstream ion gyroperiod. In the strong field regime or, equivalently, when the shock is followed for longer than a gyroperiod, the reflected ions turn around in the upstream magnetic field and gain energy from the transverse flow electric field. The upstream ions decelerate the incoming flow, thereby compressing the magnetic field to produce a foot [*Woods, 1969, 1971; Eiselevich et al., 1971*]. The energized ions transmitted through the shock on their second encounter create a superthermal ring distribution downstream.

Recent numerical simulations indicate that a self-consistent ion reflection shock can exist in a quasi-neutral plasma without Debye length substructure [*Leroy, 1983*]. Since the simulated shocks resemble typical bow shocks in several important ways, we review the physics that went into, and came out of, these simulations (section 7.2). In section 7.3, we review those bow shock data analyses which were specifically designed to test the theory of ion reflection shocks. In section 7.4, we discuss the range of parameters for which an ion reflection shock is expected.

7.2. Ion Reflection Shocks

Leroy et al. [1981, 1982] simulated perpendicular shocks using a one space dimension, three velocity space dimension hybrid code, with kinetic ions and fluid electrons. The ions and electrons interacted by means of an artificially implemented resistivity that was constant in space and time but could be varied from run to run. The resistivity was typically chosen according to standard estimates of ion sound anomalous resistivity. The simula-

tions were entirely quasi-neutral, since Debye length spatial structure was not resolved numerically. The simulation runs lasted several ion Larmor periods, and were completed before interactions with the boundaries affected the interior solution.

Understanding how *Leroy et al.* [1981, 1982] initialized their simulations is essential to understanding the formation of the ion reflection shock. The simulation box was initially divided into three regions, with the upstream and downstream Maxwellian ion plasmas and magnetic fields linked by the MHD RH relations, given specified electron-to-ion temperature ratios. These regions were connected by a thin layer in which plasma quantities varied linearly from upstream to downstream.

During the first half Larmor period of the simulation, the magnetic ramp sharpened to the magnetic Reynolds length, and some downstream ions crossed the shock. These were reflected in the upstream magnetic field. They reduced the center-of-mass velocity of the upstream ion distribution, and as they turned in the upstream magnetic field, their Lorentz field added to the longitudinal electric field E_x . Both effects contributed to the formation of a potential overshoot in the shock ramp, which effectively insulated the downstream region from the upstream region after the first half Larmor period. Although downstream ions no longer penetrated upstream, upstream ions began to be reflected from the potential in

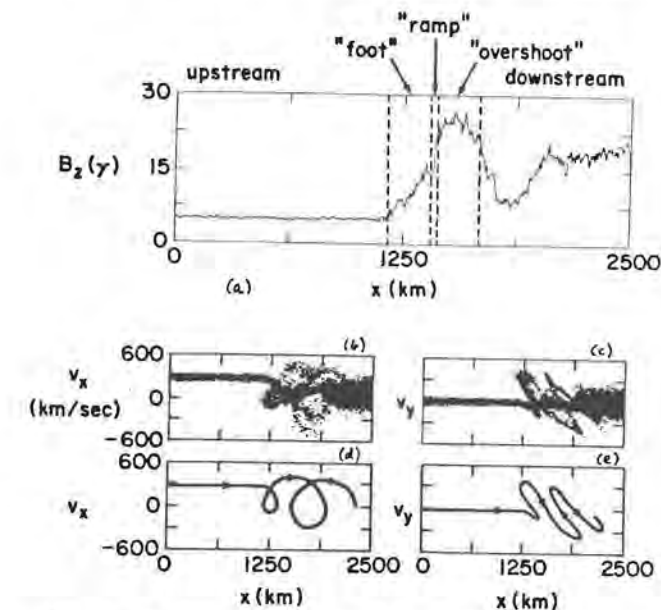


Fig. 11. An ion reflection shock simulation. The top panel shows the magnetic field magnitude for a perpendicular shock simulated by *Leroy et al.* [1982]. The foot, ramp, and overshoot are indicated. An undershoot follows the overshoot. The bottom panels present V_x - x (left) and V_y - x (right) ion phase space displays, which show the locations of individual ions (top), and schematic trajectories of reflected ions (bottom).

the shock ramp. After they were reflected, they could Larmor orbit in the direction of the flow electric field. On their next encounter with the shock, the energized ions had enough energy to overcome the potential barrier and be transmitted downstream. The number of reflected ions and the shock potential adjusted to one another so that the transmitted ions contributed enough to the downstream ion pressure to satisfy the RH relations. About 20% of the incoming ion stream was typically reflected. Cross-field currents induce substantial turbulence in two-dimensional shocks that reduces the reflected ion fraction [*Forslund et al., 1984*].

The added dissipation in supercritical ion reflection shocks occurs in the magnetic foot, where the reflected ions gain the energy required to satisfy the RH relations by free streaming in the flow electric field. This dissipation is accomplished without benefit of a diffusive viscosity or microturbulence.

Since *Leroy et al.'s* [1981, 1982] simulations were one dimensional, the transmitted ion ring distribution was stable. The instability of the ring distribution expected in higher dimensions will thermalize the ions downstream [*Papadopoulos, 1981a; Tanaka et al., 1983*]. Thus, true thermal equilibrium will be achieved only over a scale longer than that of the foot-overshoot system.

Instabilities of the foot ring distribution may heat a high-energy electron tail which escapes upstream [*Papadopoulos, 1981b*], possibly accounting for the energetic electrons observed to escape from the quasi-perpendicular zone of the bow shock. *Wu et al.* [1984] have discussed in considerable detail the various instabilities that might occur in ion reflection shocks.

7.3. Observations of Ion Reflection Bow Shocks

In this section, we summarize those bow shock data analyses which were specifically designed to test the theory of ion reflection shocks. Earlier measurements had found a second peak in the ion distribution downstream of supercritical shocks [*Montgomery et al., 1970; Formisano and Hedgecock, 1973a, b; Bame et al., 1979; Greenstadt et al., 1980*] which we now attribute to transmitted ions. *Paschmann et al.* [1981, 1982] found that about 20% of the incoming ions are reflected in the foot region.

A particularly impressive comparison between numerical simulation [*Leroy et al., 1981, 1982*] and observation, for a $\theta_{NB1} = 82^\circ$ bow shock of Alfvén Mach number 8 detected by ISEE 1 and 2 on November 7, 1977, found good agreement not only between the computed and observed amplitudes and spatial scales of the magnetic foot and overshoot, but also at the level of the ion phase space distribution. Reflected ions in the foot, a ring distribution in the overshoot, and gradual downstream ion thermalization were observed [*Schope et al., 1983*].

Livesey et al.'s [1982, 1984] statistical studies of the magnetic profiles of some 60 quasi-perpendicular bow

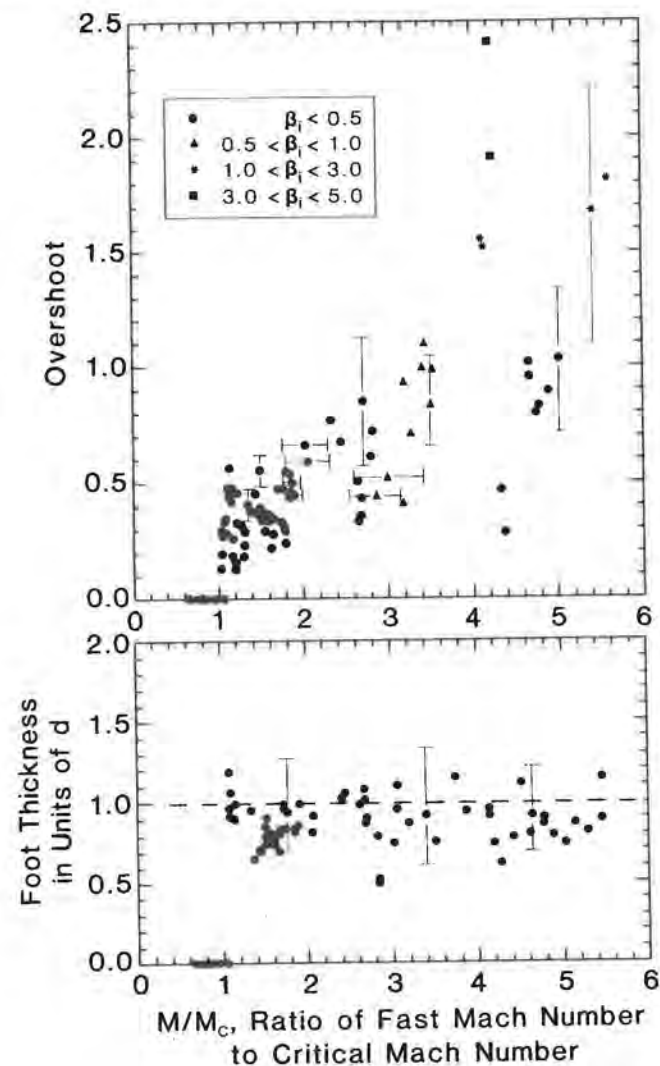


Fig. 12. Statistical studies of bow shock magnetic structure. The overshoot amplitude (top panel) and normalized foot thickness (bottom panel) are plotted as a function of the ratio of the fast Mach number to the critical Mach number M_c . The overshoot amplitude and foot normalization are defined in the text. Error bars indicate typical uncertainties in overshoot amplitude, foot thickness, and Mach number ratio [Livesey *et al.*, 1982, 1984]. Subcritical shocks have neither a foot nor an overshoot. The overshoot amplitude increases suddenly in the range $M_c < M < 1.2 M_c$. The foot thickness is independent of shock parameters when $M > M_c$.

shocks ($43^\circ < \theta_{NB1} < 88^\circ$) are summarized in Figure 12. The top panel shows the overshoot amplitude, defined as

$$A = \frac{B_m - B_2}{B_2} \quad (25)$$

where B_m is the maximum magnetic field in the overshoot and B_2 is the downstream magnetic field, as a function of the ratio of the fast Mach number to the critical Mach

number. The use of ISEE 1 and 2 measurements permitted an accurate calculation of spatial scale lengths. The bottom panel shows the dependence of the foot thickness upon the Mach number ratio. Livesey *et al.* [1984] generalized to oblique shocks Woods' [1971] and Phillips and Robson's [1972] estimate of the foot thickness for perpendicular shocks, assuming that upstream ions specularly reflect from the main shock ramp. The foot thicknesses were normalized to the distance d along the shock normal at which a reflected ion turns back to the shock. Subcritical shocks had neither a foot nor an overshoot, while supercritical shocks had both. The foot thicknesses scaled as d and were independent of Mach number and other shock parameters. The overshoot thicknesses scaled as the reflected ion Larmor radius based on the upstream magnetic field.

7.4. Parameter Space for Ion Reflection Shocks

7.4.1. *Range of θ_{NB1} .* For 90° shocks, all reflected ions are turned back into the shock. However, for oblique shocks some reflected ions recross the shock and some escape upstream, depending upon the ions' Larmor phase angles at the point of reflection. The fraction of the ions that can escape upstream increases with decreasing θ_{NB1} , and most escape for $\theta_{NB1} \leq 45^\circ$, [Phillips and Robson, 1972; Edmiston *et al.*, 1982; Leroy and Winske, 1983]. Thus, ion reflection shocks should be quasi-perpendicular, consistent with the fact that Livesey *et al.* [1984] found shocks with an overshoot and a foot only for $\theta_{NB1} \geq 43^\circ$.

7.4.2. *The second critical Mach number.* We argued section 5 that an electrostatic ion sound subshock is expected to form above the critical Mach number, yet the ion reflection shocks discussed in section 7.2 occur in a quasi-neutral plasma. In this section, we discuss the possibility that the ion sound subshock and the ion reflection shock occur in distinct Mach number ranges.

There has to be enough shock-heated ions approaching the shock surface from downstream to initiate a reflection shock. Leroy *et al.* [1982] suggested that the downstream flow speed must equal the ion thermal speed, C_{i2} , for this to happen. If so, strong ion reflections shocks set in at a second critical Mach number, defined by the condition $U_2 = C_{i2}$, which exceeds the (first) critical Mach number defined in sections 4 and 5. The second critical Mach number can only be calculated by taking into account the dissipation in the shock front, so that the downstream electron-to-ion temperature ratio, T_{e2}/T_{i2} , may be determined. We can estimate the second critical Mach number using the Rankine-Hugoniot relations if we treat T_{e2}/T_{i2} as a free parameter to be determined empirically. It is clear that the first and second critical Mach numbers approach one another as T_{e2}/T_{i2} approaches zero. Furthermore, since U_2 always exceeds $C_{S2}/5^{1/2}$ for $\gamma = \frac{5}{3}$ (and approaches $C_{S2}/5^{1/2}$ in the strong shock limit), the condition $U_2 = C_{i2}$ cannot be satisfied for $T_{e2}/4T_{i2}$ (and $\gamma_i = \gamma_e$). Figure 13 plots the dependence

SECOND CRITICAL MACH NUMBER

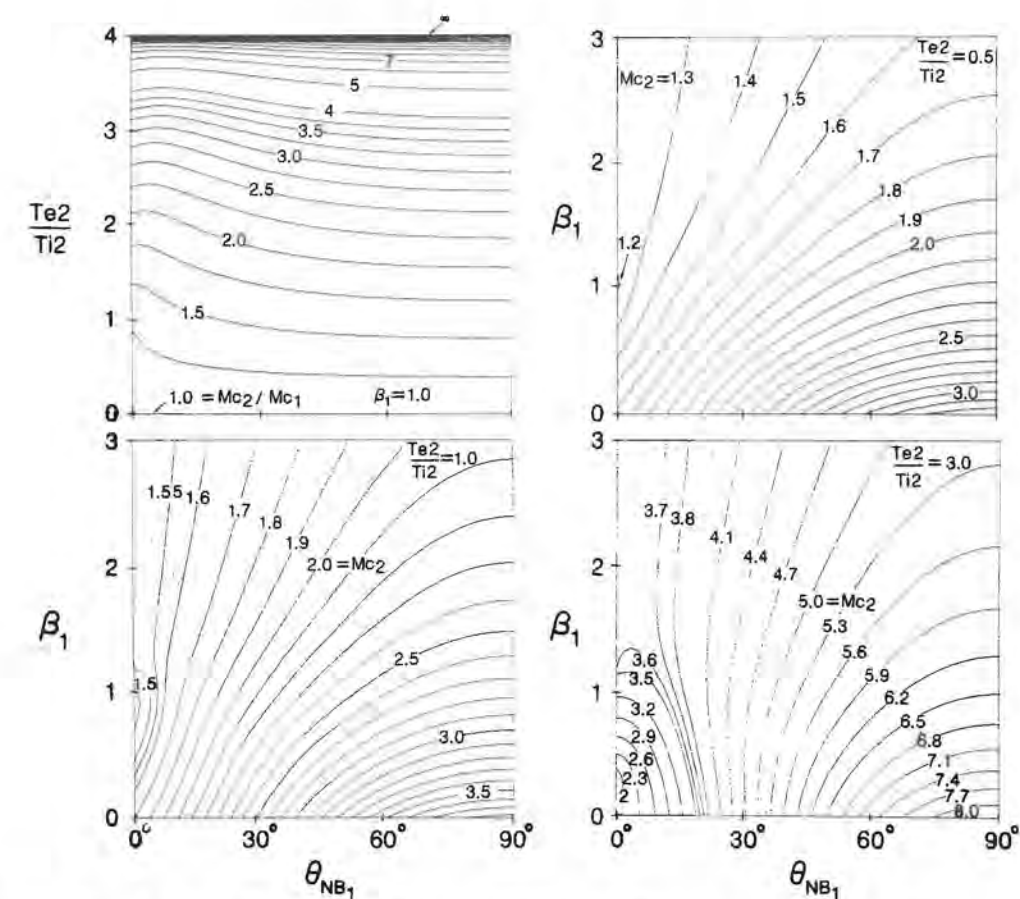


Fig. 13. Second critical Mach number. Leroy *et al.* [1982] and Manheimer and Spicer [1985] have proposed that U_2 must equal C_{i2} , the downstream ion thermal speed, for quasi-neutral, strong ion reflection shocks to occur. The upper left-hand panel contours the dependence of the ratio of the second critical Mach number to the first on the downstream electron-to-ion temperature ratio and the upstream shock normal angle, for $\beta_1 = 1$. The other three panels contour the dependence of the second critical Mach number on β_1 and θ_{NB1} for $T_{e2}/T_{i2} = 0.5, 1$, and 3.

of the second critical Mach number upon upstream shock parameters for $0 \leq T_{e2}/T_{i2} \leq 4$. The upper left-hand panel contours the dependence of the ratio of the first and second critical Mach numbers upon T_{e2}/T_{i2} and the upstream shock normal angle, for an upstream electron plus ion $\beta_1 = 1$. The other three panels contour the second critical Mach number as a function of β_1 and θ_{NB1} for $T_{e2}/T_{i2} = 0.5, 1$, and 3.

A laboratory experiment by Eiselevich *et al.* [1971] found an isomagnetic potential jump with $\sim 100\lambda_D$ scale length between the first critical Mach number and a Mach number of 4.5–5.5. This isomagnetic jump is presumably the ion sound subshock predicted by two-fluid theory. Manheimer and Spicer [1985] review other laboratory evidence for an electrostatic subshock between the first and second critical Mach numbers. These lab-

oratory experiments typically have small β_1 upstream, so that the second critical Mach number is relatively large.

The subshock is difficult to observe at the bow shock, because high time resolution potential and ion distribution functions are required. Moreover, Figure 13 shows that for typical solar wind parameters ($\beta_1 = 1$, $T_{e2}/T_{i2} = 1$), the first and second critical Mach numbers differ by about 50%, so that high-precision Mach number estimates are required to determine which regime the shock is in. Eiselevich [1982] has reviewed the bow shock evidence favoring the existence of the ion sound subshock.

Manheimer and Spicer [1985] argue that the dissipation between the first and second critical Mach numbers is due to "longitudinal resistivity," basically, that the ion and electron flow velocities parallel to the shock

normal are coupled by an interaction with the ion sound subshock that amounts to Landau damping in the small-amplitude limit. At the second critical Mach number, the electrostatic subshock is completely damped, and the ion reflection shock is essentially quasi-neutral. While some reflected ions are expected between the two critical Mach numbers, ion reflection is strong enough to dominate the dissipation only above the second critical Mach number.

7.4.3. A third critical Mach number? A heuristic argument suggests that ion reflection cannot supply all the dissipation needed for steady high Mach number shocks. The internal energy density approaches a limit of $\frac{1}{2}$ of the upstream flow energy density downstream of strong shocks (assuming $\gamma = \frac{5}{3}$). The state downstream of ion reflection shocks consists of heated electrons, a fraction $(1 - \alpha)$ of compressed thermal ions, and a fraction α of gyrating ions with speeds of about 1.7 times the upstream flow speed. Assuming that well above the second critical Mach number most of the downstream energy resides in the gyrating ions, the energy density downstream would be about $1.5 \alpha \rho_1 U_1^2$. Thus, α must exceed $\frac{2}{3}$ for the strong shock limit to be satisfied. However, simulations [Leroy et al., 1981, 1982], laboratory experiments [Chodura, 1975], and bow shock observations [Pashmann et al., 1981] all find that α , which presumably is self-consistently regulated, is roughly 0.2. Furthermore, simulations [Leroy et al., 1981, 1982; Forsslund et al., 1984] also indicate that the ion reflection shock becomes unsteady beginning at Alfvén Mach numbers of 12 or 13, at least on the spatial scale treated by the computations.

The above arguments imply that there might exist a third critical Mach number, above which ion reflection cannot provide all the needed dissipation. If we could calculate the dependence of the properties of downstream reflected ions on upstream plasma parameters, evolutionary arguments would permit us to estimate the third critical Mach number. The phase speed of a long-wavelength sound wave would be the sound speed calculated using the sum of the $\gamma = 2$ reflected ion and the $\gamma = \frac{5}{3}$ thermal pressures downstream. As such a wave steepens to the reflected ion Larmor radius, its phase speed should decrease to the thermal sound speed. Thus, the third critical Mach number should be defined by equating the downstream flow speed to the sound speed based upon the thermal pressure alone.

8. Bow Shock and Interplanetary Shock Observations

8.1. Introductory Remarks

Observational studies of the dependence of bow shock structure, and of the region upstream of the bow shock, on solar wind parameters have shown that the magnetic profiles of quasi-parallel shocks are much broader and more disorderly than any quasi-perpendicular profile. Their magnetic field appears to pulsate between up-

stream and downstream values on spatial scales that are a significant fraction of an earth radius [Greenstadt et al., 1970]. It is often difficult using magnetic data alone to determine where the quasi-parallel "shock" is, since the shock turbulence blends imperceptibly into the low-frequency waves that are found upstream on field lines that connect to the "shock surface." In sections 8.2 and 8.3, we discuss the relationship between the waves and the superthermal particles upstream and the local bow shock parameters, and the organization of the observations by the foreshock concept. The relationship between quasi-parallel shock parameters and the upstream region is obscured by the fact that the foreshock thickness is comparable with the radius of curvature of the bow shock. However, in section 8.4, we argue that recent studies of interplanetary shocks, which have much larger radii of curvature, indicate without ambiguity that foreshocks are inherent to quasi-parallel shock structure (section 8.4).

8.2. The Earth's Foreshock

As early as 1968, we knew that the solar wind can have foreknowledge of an impending shock crossing, when it is connected magnetically to the shock [Asbridge et al., 1968; Fairfield, 1969]. It seemed at first that the fast particles escaping along field lines, and the MHD waves they generate, were energetically insignificant tracers that gently signaled connection to the bow shock. When we realized that they are important parts of shock structure, the most fundamental conception of the fluid description of shocks—that no hydromagnetic signal propagates upstream—was compromised.

The most important new concept arising from the study of the magnetically connected upstream region is that of the "foreshock" [Greenstadt, 1975, 1976a, b]. If the solar wind and its magnetic field were uniform and steady, it would be easy to identify the field line that is tangent to the bow shock which defines the leading edge of the foreshock. However, because the solar wind is variable, it is laborious indeed to relate upstream observations to the instantaneous foreshock. Nonetheless, the labor has yielded rich rewards which are summarized in the beautiful picture drawn by Tsurutani and Rodriguez [1981] for an ideal gardenhose interplanetary field interacting with a steady bow shock (Plate 2). Upstream of the foreshock, all disturbances do seem intrinsic to the solar wind. Particles originating at the shock are only found downstream of the foreshock's leading edge. Given the speeds with which particles escape along field lines and the solar wind speed, simple kinematics successfully predicts where each velocity class of particle ought to be found. There is an electron (yellow) and an ion (red) foreshock. Because electrons move faster than ions parallel to the magnetic field, the electron foreshock stands upstream of the ion foreshock, and the most energetic electrons are found closest to the field line that is instantaneously tangent to the bow shock.

The electron and ion velocity distribution functions evolve progressively with distance downstream from the leading edge of their individual foreshocks, and different plasma and hydromagnetic waves are uniquely associated with the particle distributions characteristic of each region [Greenstadt et al., 1984]. Field-aligned beams of energetic electrons are found nearest the leading edge of the foreshock [K. Anderson, 1968, 1969; Feldman et al., 1973, 1983; K. Anderson et al., 1979; R. Anderson et al., 1981]. The energetic electron angular distributions become progressively more diffuse with distance downstream of the foreshock, and the typical energies decrease in a pattern consistent with the sweeping back of electron trajectories by the solar wind electric field [Anderson et al., 1979]. At lower energies, the electron heat flux in the foreshock is often directed upstream away from the bow shock, reversing the normal direction of the solar wind electron heat flux.

The spatial evolution of the foreshock ion distribution mirrors that of the electrons. Few keV field-aligned beams are found at the leading edge of the ion foreshock. Further downstream, so called "intermediate" ion distributions are spread in energy and pitch angle [Gosling et al., 1980; Bonifazi and Moreno, 1981a, b] which extend to energies of several hundred keV [Scholer et al., 1979; Ipavich et al., 1981a, b], comparable with the energies achieved by Fermi acceleration in interplanetary shocks [Lee, 1983a]. Phase-bunched "gyrating" ion beams are often observed deep within the foreshock [Gurgiolo et al., 1981; Eastman et al., 1981].

The upstream superthermal ion energy density can exceed that of the interplanetary field by as much as a factor 5 [Ipavich et al., 1981a]. More significantly, the solar wind is decelerated and deflected when it enters the ion foreshock [Bonifazi et al., 1980] by an amount compatible with the momentum flux carried by shock escaping ions [Bame et al., 1980; Sentman et al., 1981a]. Since part of the overall shock transition is accomplished in the foreshock, the foreshock is part of shock structure.

The superthermal particles generate a rich spectrum of plasma waves in the foreshock [Scarf et al., 1970, 1971]. Escaping electrons generate electron plasma waves [Scarf et al., 1971; R. Anderson et al., 1981; Etcheto and Faucheux, 1984], low-frequency (~ 1 Hz) whistler waves [Feldman et al., 1983; Sentman et al., 1983], and higher-frequency whistlers [Fairfield, 1974; Tokar et al., 1984]. Broadband 0.5–5 kHz electrostatic fluctuations, whose frequency is consistent with Doppler-shifted ion sound waves, are associated with both superthermal ions and electrons [Scarf et al., 1971; Rodriguez and Gurnett, 1975; R. Anderson et al., 1981; Parks et al., 1981; Fuselier and Gurnett, 1984]. However, there is no definite proof that the measured particle distributions are unstable to ion sound waves.

It is important to both shock structure and particle acceleration theories that large-amplitude long-wavelength ($\sim 1 R_E$) hydromagnetic waves are associated

with ions escaping from the bow shock. Transverse MHD waves are found in the ion beam region [Hoppe et al., 1982], and steepened, more compressional waves achieve large amplitudes ($\Delta B/B \sim O(1)$) in the diffuse proton zone [Greenstadt et al., 1968; Fairfield, 1969; Paschmann et al., 1979; Greenstadt et al., 1980; Hoppe et al., 1981].

The upstream ions appear to generate the large-amplitude low-frequency waves in the earth's foreshock, as Barnes [1970] first suggested. Gary [1981], Gary et al., [1981], and Sentman et al. [1981b] have shown for several specific examples that the measured ion distributions are unstable to MHD waves of the observed wavelength and polarization. Thus, the ions propagate upstream and generate waves which are then blown back towards the shock by the solar wind.

8.3. Relationship Between Upstream Phenomena and Local Bow Shock Parameters

The kinematic mapping arguments which led to the foreshock model shown in Plate 2 relate the orderly progression of the electron and ion distributions to the local shock normal angle at the point where the particles first escape upstream. The energetic electron and ion beams originate from the quasi-perpendicular zone of the bow shock. Energetic electrons can be accelerated by instabilities generated by the reflected ions in the magnetic foot of a supercritical quasi-perpendicular shock [Papadopoulos, 1981b]. Furthermore, as the downstream ion ring distribution is thermalized and isotropized, some energetic ions will be scattered onto trajectories that reintersect the curved bow shock surface from behind. Those ions that cross that shock can form the ion beams that are observed to stream from the quasi-perpendicular zone of the bow shock [Tanaka et al., 1983].

The diffuse distributions certainly appear to escape from the quasi-parallel zone of the bow shock. However, because of an inherent ambiguity, earth foreshock measurements cannot conclusively settle whether the apparent difference between quasi-perpendicular and quasi-parallel shocks is fundamental. It has been argued that many of the diffuse ions come from the ion foreshock beam [Bame et al., 1980; Bonifazi and Moreno, 1981b]. As the beam propagates upstream, it destabilizes low-frequency hydromagnetic waves which subsequently scatter and decelerate the beam ions. The decelerated ions and the waves are blown back into the quasi-parallel zone of the bow shock surface. If there are enough of them, they may possibly account for the disordered magnetic structure and diffuse ion distribution that are observed. In this interpretation, the quasi-parallel structure we observe is an artifact of the small radius of curvature of the bow shock. On the other hand, Edmiston et al. [1982] argued that shock-heated ions ought to escape upstream from plane quasi-parallel shocks, in which case the observed structure is intrinsic to quasi-parallel shocks. Whatever the situation, the curvature of the bow shock does alias the results, so that it is difficult to

assign uniquely the phenomena observed upstream to a particular shock normal angle. Nonetheless, it appears that the quasi-parallel, quasi-perpendicular transition occurs suddenly near $\theta_{NB1} = 45^\circ - 50^\circ$.

The large-amplitude waves upstream also blur the relationship between waves and particles and the parameters of the bow shock. For example, when the local shock normal angle based on the averaged upstream magnetic field is near 45° , the instantaneous shock normal angle may oscillate between the quasi-perpendicular and quasi-parallel regimes, thereby making the local shock structure and the distribution of escaping particles unsteady [Greenstadt, this volume].

8.4. Structure Upstream of Interplanetary Shocks

Since their radii of curvature are 250–2500 times larger than the bow shock's, interplanetary shocks should reveal what is intrinsic to quasi-parallel structure. However, detections of the classical foreshock signatures—superthermal ions and magnetohydrodynamic waves—hours before an interplanetary shock have been difficult to relate to the shock, not only because the solar wind normally has energetic ions and is magnetically turbulent, but also because the global shock and interplanetary field geometry is difficult to ascertain. Our increasingly complete understanding of bow shock upstream phenomenology has helped to clarify the shock association, since MHD turbulence that is accompanied by other upstream signatures can now be related to interplanetary shocks.

The first evidence that quasi-parallel interplanetary shocks have large foreshocks came from a study of upstream ion sound fluctuations [Kennel et al., 1982]. Ion sound fluctuations, whose spectrum was similar to that upstream of the bow shock, extended hundreds of earth radii upstream of quasi-parallel interplanetary shocks. They were not found upstream of quasi-perpendicular interplanetary shocks. Shortly thereafter, magnetometer studies [Russell et al., 1983; Tsurutani et al., 1983; Kennel et al., 1984a, b; Vinas et al., 1984] revealed that MHD waves similar in period and amplitude to those upstream of the bow shock occur upstream of quasi-parallel interplanetary shocks. The measurements of superthermal electrons and ions upstream of interplanetary shocks have been discussed by Gosling et al., [1983, 1984] and Tsurutani and Lin [1985]. Thus, it appears that a foreshock is intrinsic to quasi-parallel shocks.

9. Quasi-Parallel Shocks

9.1. Theories of Parallel Shocks

The first parallel shock theory [Parker, 1961] visualized the shock layer as consisting of two counterstreaming ion beams which would be firehose unstable when the upstream β_1 is high—a remarkably prescient forecast.

The first parallel shock theory to incorporate classical steepening arguments is due to Moiseev and Sagdeev

[1963]. When $C_s^2/C_A^2 > 1$, the parallel fast mode is an ion sound wave which will steepen until it reaches Debye length scales. Reflection of upstream ions would then lead to an irreversible ion sound wave train which accomplishes the shock transition. Moiseev and Sagdeev [1963] went on to argue that, in the absence of collisions, shock compression would increase only the temperature parallel to the magnetic field, so that if β_2 were high enough, a firehose instability would grow on the downstream thermal anisotropy. This suggestion motivated Kennel and Sagdeev [1967], Kennel and Petschek [1968], Berezin and Sagdeev [1969], and Galeev and Sagdeev [1970] to develop a theory of low Mach number parallel firehose shocks in very high β plasmas (see also Sagdeev [1979]). At low Mach numbers, relaxation of the ion anisotropy through the growth of Alfvén waves can provide for a shock transition. Auer and Volk's [1973] numerical calculations confirmed the general features of this theory, but indicated that an ion sound subshock was required at higher Mach numbers [Jackson, 1983]. A recent simulation of a 10° shock with an Alfvén Mach number of 4 showed that the downstream thermal anisotropy relaxed to firehose marginal stability via the growth of Alfvén waves [Kan and Swift, 1983] but, because the code assumed quasi-neutrality, could not have found an electrostatic substructure.

The above firehose shock models do not pay attention to upstream structure, either a standing whistler wave train [Kan and Swift, 1983; Quest et al., 1983] or the injection of energetic particles into the foreshock. Lee [1982, 1983a] considered the idealized case in which a thin, parallel planar, shock injects a monoenergetic ion beam into a broad foreshock. He then computed the growth rate of parallel propagating Alfvén waves by the resonant analog of the firehose instability [Kennel and Scarf, 1968], the spatial decay of the ion beam due to quasi-linear pitch angle scattering, and the subsequent ion Fermi acceleration by shock compression. Lee's [1982, 1983a] theory is the foreshock analog of the firehose shock models discussed above.

In summary, nearly, all theories of quasi-parallel shock structure agree that long-wavelength MHD turbulence is central to the dissipation in both the shock and foreshock.

9.2. Escape of Superthermal Ions Upstream of Quasi-Parallel Shocks

The fact that quasi-parallel shocks allow significant access upstream of ions that have interacted with the shock seems to be their primary observational characteristic, since the upstream waves can be derived from the ions. The types of ion distributions observed upstream—"reflected," "intermediate," "diffuse"—reflect both how they are generated and how they interact with upstream turbulence, and sophisticated studies are presently under way to unravel these detailed interrelationships [Schwartz et al., 1983].

DISPERSIVE WAVE TRAINS

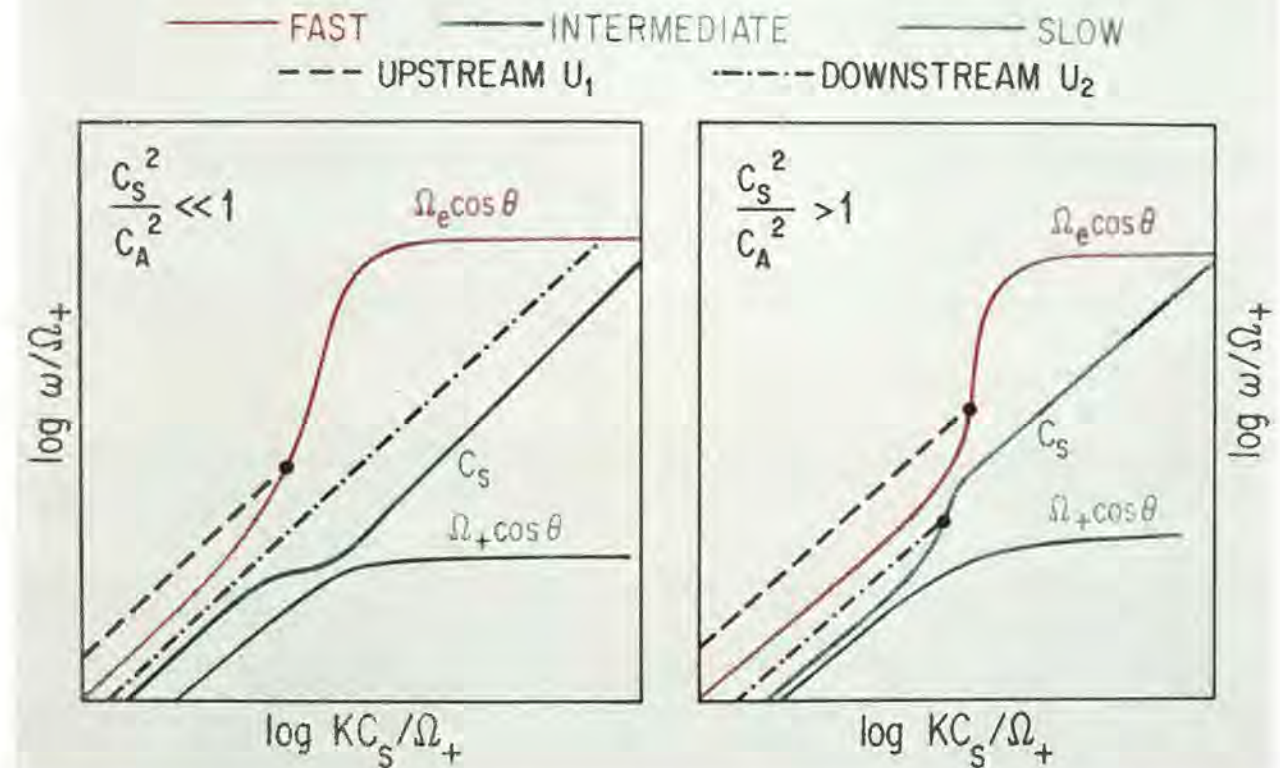


Plate 1. The two-fluid quasi-neutral dispersion relation for oblique propagation. The left-hand and right-hand panels sketch the two-fluid quasi-neutral dispersion relation obtained by Formisano and Kennel [1969] for $C_s^2 < C_A^2$ and $C_s^2 > C_A^2$, respectively. The fast, intermediate, and slow branches are indicated by red, blue, and green lines, respectively. The dashed and dash-dotted lines indicate the flow speed upstream of fast shocks (both panels) and downstream of subcritical (left) and supercritical (right) shocks, respectively. In principle, a whistler wave can stand upstream of both $C_s^2 < C_A^2$ and $C_s^2 > C_A^2$ oblique shocks. When the shock is subcritical (left), an almost electrostatic wave on the whistler resonance cone can phase-stand downstream. It is possible for a dispersive mode on the intermediate branch to phase-stand downstream of supercritical shocks. A Debye length structure (not included in the right-hand panel) might also be part of the downstream structure of supercritical oblique shocks.

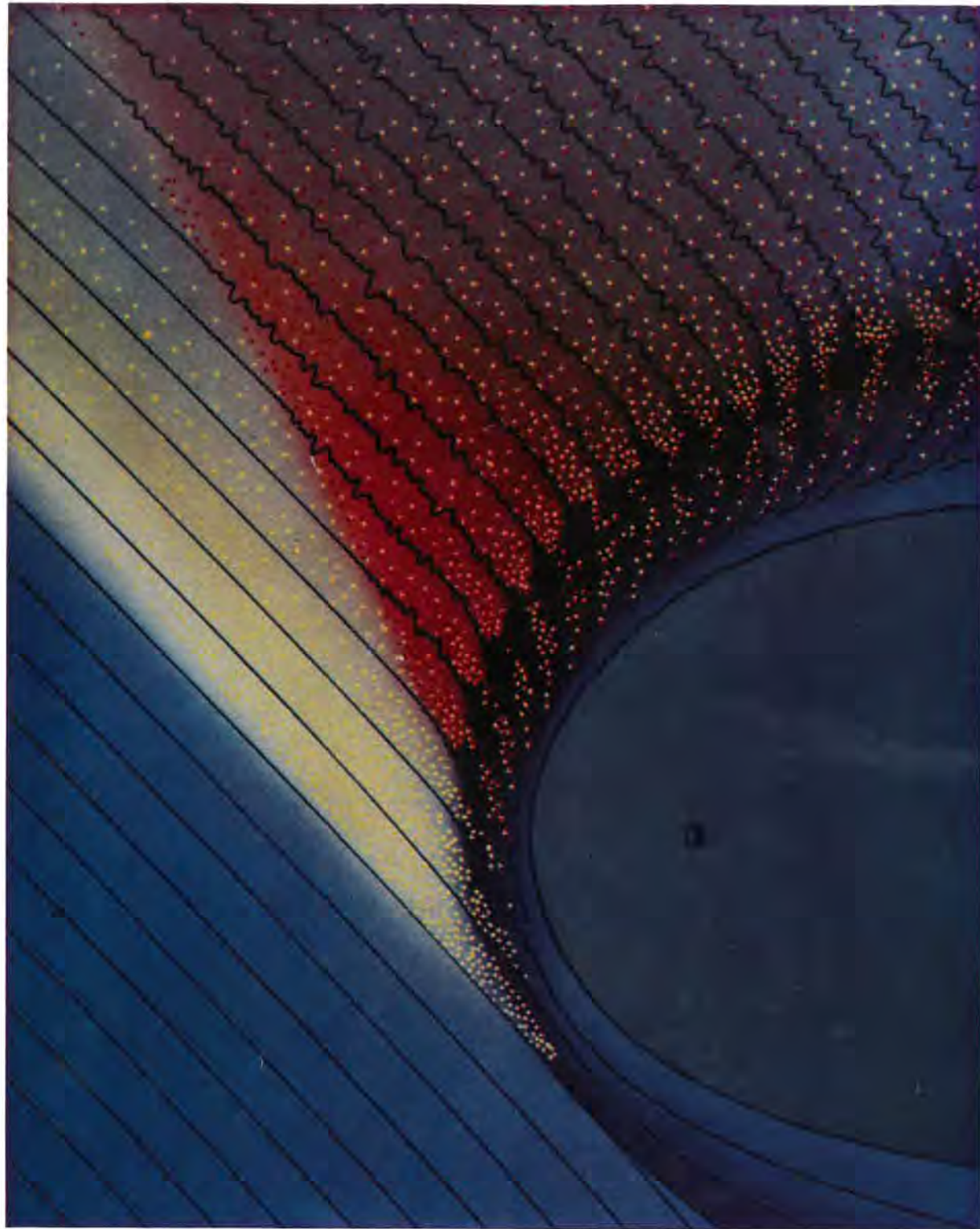


Plate 2. Foreshock schematic [Tsurutani and Rodriguez, 1981]. Energetic electrons escape upstream from the quasi-perpendicular zone of the bow shock (yellow) near the point of tangency between the upstream magnetic field (solid blue lines) and the bow shock. Superthermal ions (red) escape upstream from the quasi-perpendicular zone of the bow shock, but because they propagate more slowly than electrons, the leading edge of the ion foreshock is downstream of the leading edge of the electron foreshock. Large-amplitude, long-wavelength MHD waves are found downstream of the ion foreshock's leading edge.

FORESHOCK CRITICAL ANGLE FORESHOCK CRITICAL MACH NUMBER

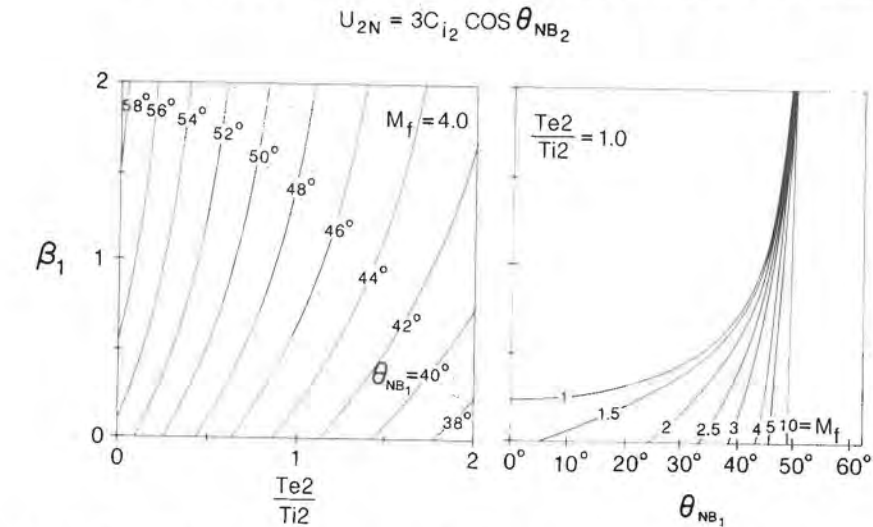


Fig. 14. Foreshock critical Mach number and angle. The right-hand panel contours the dependence of the upstream Mach number for which $U_2 = 3C_{i2} \cos \theta_{NB2}$ on the upstream β_1 and shock normal angle θ_{NB1} , assuming $T_{e2}/T_{i2} = 1$ downstream. To the right and below each curve, the flux of downstream escaping ions will be small. For the Mach number range appropriate to the bow shock, the escaping flux turns on at a critical shock normal angle. The left-hand panel contours the dependence of this critical shock normal angle upon the upstream β_1 and the downstream T_{e2}/T_{i2} , for an upstream fast Mach number of 4. The critical shock normal angle depends weakly on β_1 and somewhat more strongly on T_{e2}/T_{i2} .

We have already pointed out that when the upstream shock normal angle is less than 45° , most reflected ions escape upstream. However, quasi-parallel shocks also cannot confine heated ions downstream. A downstream ion can free stream along the magnetic field and catch the shock if its parallel velocity V_{\parallel} satisfies $U_2 = V_{\parallel} \cos \theta_{NB2}$, when θ_{NB2} is the downstream shock normal angle. Edmiston *et al.* [1982] estimated the superthermal ion flux upstream by assuming that shock-catching ions are transmitted back through the shock, conserving their magnetic moments. The upstream fluxes will be maintained if the loss region in the downstream ion phase space is continuously refilled by wave-particle scattering. It is clear that no particles can escape upstream of a perpendicular shock, and that the escaping flux will increase with decreasing upstream shock normal angle. Edmiston *et al.* [1982] found that near $\theta_{NB1} \approx 45^\circ$ the flux of upstream ions suddenly becomes comparable to that observed. Thus, this mechanism can account for the rapid change between quasi-parallel and quasi-perpendicular behavior.

To conform to the spirit of this paper, we will construct a "foreshock critical Mach number," at which significant fluxes of downstream ions are expected to escape upstream. The condition $U_2 = 3C_{i2} \cos \theta_{NB2}$ defines a rough threshold Mach number at which the number of shock-catching ions becomes significant. The right-hand panel of Figure 14 contours the dependence of the foreshock critical Mach number upon the upstream β_1 and shock

normal angle, assuming $T_{E2} = T_{i2}$ downstream. To the right of each curve, U_2 will exceed $3C_{i2} \cos \theta_{NB2}$, and the escaping flux will be small. For the Mach number range appropriate to the bow shock, the escaping flux turns on at a critical shock normal angle. The left-hand panel of Figure 14 contours the dependence of this critical shock normal angle upon the upstream β_1 and the downstream T_{e2}/T_{i2} , assuming the upstream fast Mach number is 4.

A more sophisticated view of the ion transport across the shock has been put forth by Eichler [1979] and Ellison, [1981], who argued that the scattering mean free path is proportional to the ion Larmor radius and is therefore energy dependent. In such a case, we would observe the low-energy ion "temperature" to jump across a thin "shock," whereas we would find that energetic ions free stream through the "shock" and only scatter upstream and downstream. Far upstream, we would divide the ion distribution into a low-energy part and a distinct superthermal component. The entire region would be filled with hydromagnetic waves over the broad wavelength range required to resonate with both thermal and superthermal ions.

10. Shock Acceleration of Energetic Particles

10.1. Interaction of Single Particles With Shocks

Until recently, most theories of cosmic ray acceleration concentrated on elucidating how single particles can attain high energy by single or multiple encounters

with collisionless shocks which are considered to be infinitely thin and whose plasma structure is therefore assumed to be relatively unimportant. Looked at in this fashion, shocks can accelerate particles in several ways. Ions whose Larmor radius exceeds the shock thickness conserve their gyrophase-averaged magnetic moment [Chen and Armstrong, 1972; Shabanskii, 1962; Pesses, 1979; Terasawa, 1979a, b; E. N. Parker, unpublished manuscript, 1958]. Such ions approaching the shock from upstream would therefore be either reflected from or transmitted through the jump in magnetic field and potential at the shock, depending upon their pitch angle. Reflected ions grad- B and curvature drift parallel to the flow electric field and thereby acquire energy, the more efficiently the more quasi-perpendicular the shock [Sonnerup, 1969]. However, since multiple reflections are needed to account for the higher-energy particles accelerated by interplanetary shocks [Pesses, 1979], reflected ions must be scattered from upstream MHD turbulence back towards the shock. They then can be either re-reflected or retransmitted at their next encounter with the shock. Re-reflected particles can repeat the above cycle, and some can reach high energy.

Energetic particles that are transmitted through the shock can be scattered by downstream magnetic turbulence back toward the shock. Such particles are subject to first-order Fermi acceleration by multiple reflections between upstream and downstream waves that convect approximately with the local flow speed [Fisk, 1971]. The shock then serves primarily to decelerate the flow so that the scattering centers appear to converge toward one another in the shock frame. The integral spectrum for particles Fermi-accelerated by infinite plane shocks depends only upon the ratio of upstream and downstream flow speeds [Krimsky, 1977; Axford et al., 1971; Bell, 1978a, b; Blandford and Ostriker, 1978; Lee, 1982, 1983a]. Because the calculated spectral index is close to the observed galactic cosmic ray index, supernova shocks are promising candidates to accelerate galactic cosmic rays [Axford, 1981]. In the test particle limit, this mechanism does not take into account the momentum transfer between cosmic rays and the plasma which decelerates the upstream flow.

10.2. Tests of Fermi Acceleration Theory

For the solar system, first-order Fermi acceleration theory has been applied to the diffuse ions upstream of the bow shocks [Terasawa, 1979a, b, 1981; Eichler, 1981; Lee et al., 1981; Forman, 1981; Ellison, 1981; Lee, 1982], and to energetic solar particle (ESP) events, in which energetic ions increase smoothly upstream of interplanetary shocks [Scholer and Morfill, 1975; Scholer et al., 1983; Lee, 1983a]. Lee's [1982] theory predicts the energy spectra of different species reported by Ipavich et al. [1981a] and the spectrum and amplitude of the low-frequency waves observed upstream of the bow shock by Hoppe et al. [1981] and others. The spectrum of bow

shock diffuse particles cuts off above about 100 keV, a fact which may be explained by the finite extent of the bow shock. Either a given magnetic field line remains connected to the region where the bow shock is strong for a finite time, or the particles diffuse across the magnetic field onto field lines which no longer interact with the shock [Eichler, 1981; Skadron and Lee, 1982]. Either effect limits the number of shock crossings a particle can have and, therefore, the energy to which it can be accelerated.

The field line connection time is larger for interplanetary shocks than for the bow shock, so the first-order Fermi mechanism will have longer to operate. The energetic ion fluxes theoretically should increase exponentially, approaching a steady, planar shock, maximize at the shock, and hold approximately constant downstream—features characteristic of ESP events. The accelerated ions should be, and are, essentially isotropic in the shock frame upstream and isotropic in the solar wind frame downstream.

There have been relatively few measurements of moderate-energy ions in ESP events in the energy range (tens of keV) that bridges the low-energy plasma and high-energy cosmic rays (however, see Lin et al. [1974], Gosling et al. [1980, 1981, 1983, 1984]). A recent study of 30–150 keV/Q protons and alphas in three ESP events [Scholer et al., 1983] finds that the particle energy and angular distributions and spatial profiles are consistent with first-order Fermi acceleration theory.

Lee [1983a] applied his foreshock model to the November 12, 1978, interplanetary shock, which was a quasi-parallel (41°) shock with a fast Mach number of 2.7 [Kennel et al., 1984b]. Starting with Scholer et al.'s [1983] measured 30 keV/Q ion intensity, Lee [1983a] accounted for the ion intensity and spectrum up to 200 keV and predicted an Alfvén wave amplitude in good agreement with observation [Kennel et al., 1984a, b].

10.3. Correlations of the Properties of Accelerated Particles With Shock Parameters

Lee and Fisk [1982] and Lee [1983b] have reviewed the association of energetic particles and shocks in the heliosphere. Interplanetary shocks near 1 AU are accompanied by ESP events [Klecker et al., 1981], "shock spike" events [Sarris and Reinhard, 1981], and "postshock enhancements" [Gosling et al., 1980]. As mentioned above, ESP events are upstream ion enhancements extending to energies of a few MeV occurring for a few hours prior to shock passage. Shock spike events are impulsive ion enhancements (0.1–1 hour) occurring at the time of shock encounter. In this section, we concentrate on recent studies that relate the properties of accelerated particles to shock parameters.

Interplanetary shocks as a class comprise subcritical and supercritical shocks, quasi-parallel and quasi-perpendicular shocks. They may be generated by the quasi-steady interaction of fast and slow solar wind

streams, or by impulsive motions in the solar corona. The energetic particle profiles associated with them are correspondingly diverse [Van Nes et al., 1984]. Van Nes et al. [1984] and Tsurutani and Lin [1985] found that quasi-perpendicular and quasi-parallel shocks are responsible for shock spike and ESP events, respectively. The largest energetic proton fluxes are generally produced by oblique but definitely quasi-parallel shocks [Van Nes et al., 1984]. It is not clear if the accelerated particle intensity changes at the first (or second) critical Mach number.

Mitchell and Roelof [1983] have shown that the probability of observing a 50–200 keV ion flux above a given threshold intensity upstream of the earth's bow shock increases exponentially with $\cos \theta_{NB1}$, where θ_{NB1} is the shock normal angle on the field line connecting the spacecraft to the bow shock. The highest peak intensities are also observed for quasi-parallel connection. The peak intensities at the bow shock are about an order of magnitude smaller than those associated with strong quasi-parallel interplanetary shocks.

In summary, the distinction between quasi-parallel and quasi-perpendicular shocks is beginning to emerge from recent studies of energetic particles associated with interplanetary shocks. Quasi-parallel shocks appear to produce the largest fluxes of diffusively accelerated protons.

10.4. Self-Consistent Foreshock Models

E. N. Parker (unpublished manuscript, 1958) first realized that if interstellar shocks do accelerate the observed galactic cosmic rays, it follows that cosmic rays have sufficient energy density to contribute to shock structure. The test particle limit discussed in section 10.1 may therefore be misleading. Wentzel [1971], Axford et al. [1977, 1982], and Drury and Volk [1981] included the pressure, but not the number and momentum densities, of the cosmic rays in the calculation of the structure of shocks in an unmagnetized plasma. They assumed that cosmic rays diffuse spatially with a long characteristic scale length, and that the thermal plasma is subject to unspecified dissipation due to microturbulence. Their calculations retrieve the gas dynamic jump conditions when no energetic particles are present. On the other hand, if the upstream cosmic ray pressure is nonzero and the sonic Mach number exceeds about 10, the entire shock transition takes place in the cosmic rays without a discontinuity in the thermal plasma. For lower sonic Mach numbers, there must be both a cosmic ray foreshock and a local plasma subshock—the situation which should pertain to typical solar system shocks.

We have generalized Drury and Volk's [1981] gas dynamic calculations to magnetohydrodynamics, to illustrate the dependence of subshock properties on shock normal angle. At the subshock critical Mach number, the downstream flow speed equals the fast MHD speed based upon the plasma pressure, excluding the cosmic ray pressure. Each quadrant of Figure 15 plots a different proper-

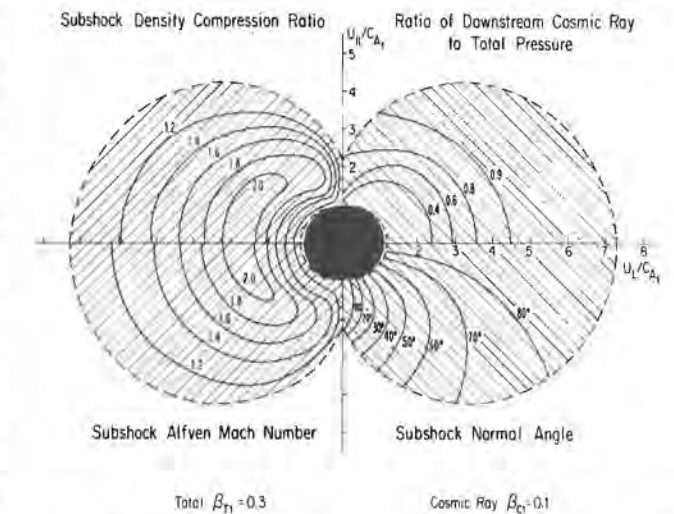


Fig. 15. MHD cosmic ray subshocks. This figure presents our generalization of Drury and Volk's [1981] gas dynamic calculation to MHD. The upstream total β_{T1} and energetic particle β_{c1} are 0.3 and 0.1, respectively. Each quadrant represents a different property of the subshocks which are expected in the hatched regions between the dashed curves, which indicate the upper and lower critical Mach numbers. A plasma observer would call the subshock the shock itself. The radial coordinate is the Alfvén Mach number, and the angular coordinate is the shock normal angle. The subshock density compression ratio (top left quadrant) and Alfvén Mach number (bottom left) are reduced, because part of the RH relations are satisfied in the cosmic ray foreshock. Similarly, magnetic field refraction in the foreshock increases the subshock normal angle relative to that of the entire structure (lower right). The ratio of downstream cosmic ray to total pressure is probably an overestimate.

ty of that subshock expected when the total plasma plus cosmic ray β_{T1} upstream is 0.3, and the upstream cosmic ray β_{c1} is 0.1. Energetic particle scattering can provide all the dissipation for very weak and very strong shocks. Thus, there are upper and lower critical Mach numbers (dashed curves) between which plasma subshocks are required (shaded). The left-hand quadrants contour the subshock Alfvén Mach number and density compression rate, and the lower right quadrant contours the local subshock normal angle. Since the flow is decelerated in the foreshock, the subshock is weaker than it would be in the absence of energetic particle scattering, and part of the magnetic field refraction required by the Rankine-Hugoniot relations occurs in the foreshock. The upper right quadrant contours the ratio of the cosmic ray pressure to the total particle pressure downstream.

Our oversimplified computations assume that the MHD turbulence needed to scatter energetic particles exists upstream of all shocks, rather than just quasi-parallel shocks. They do not include the Alfvén wave energy density in the conservation laws used to determine the properties of the subshock [McKenzie and Volk, 1982;

COLLISIONLESS SHOCK FRIEDRICHS DIAGRAM

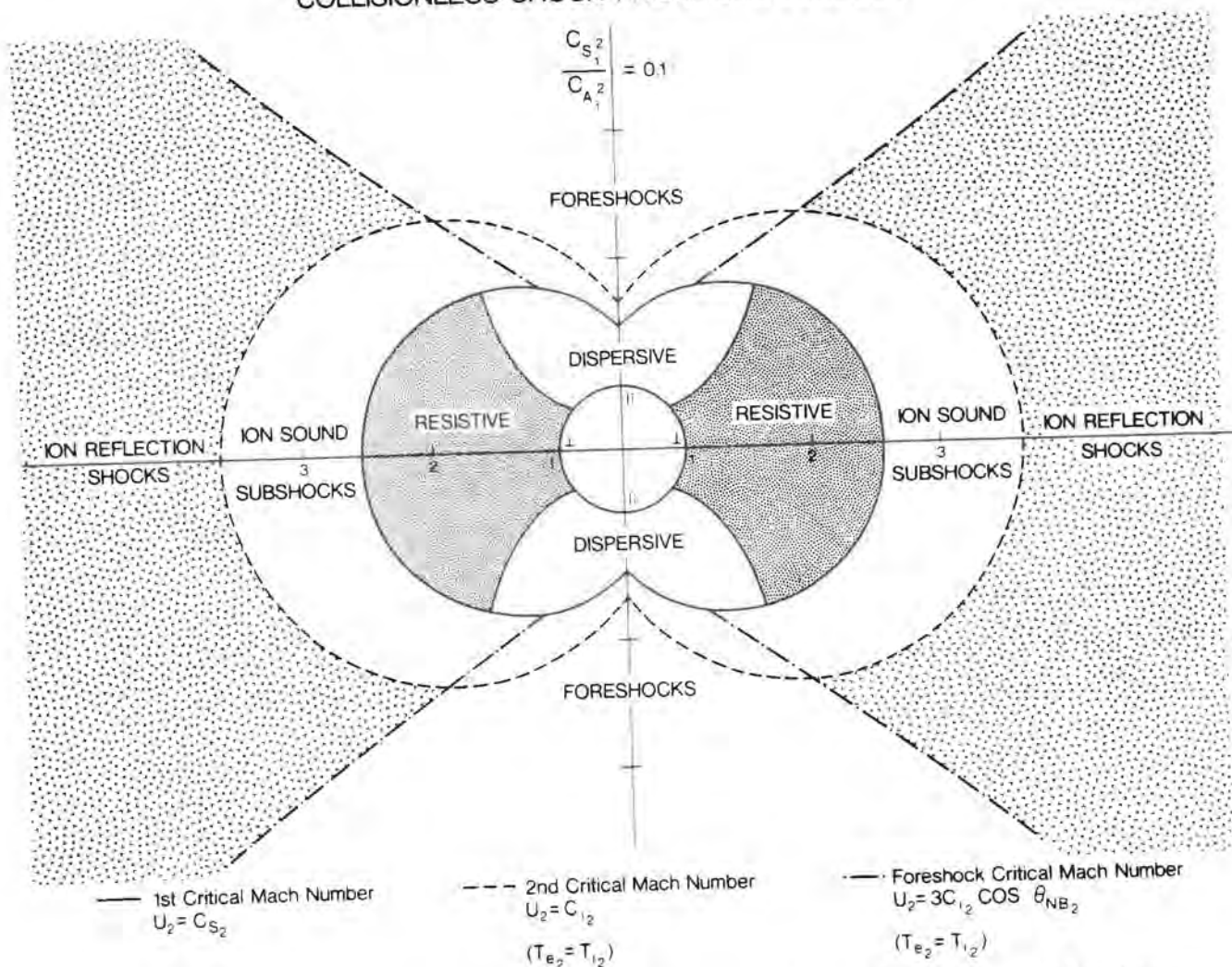


Fig. 16. Collisionless shock Friedrichs diagram. Shown here, for $C_S^2 = 0.1 C_A^2$ upstream, are the dependence upon the upstream shock normal angle of the first (solid lines), second (dashed), and foreshock (dot-dashed) critical Mach numbers, and the ion sound resistive-dispersive transition for subcritical shocks. We assumed $T_{e2} = T_{i2}$ in computing the second and foreshock critical Mach numbers. The radial coordinate is the fast Mach number, and the angular coordinate is the shock normal angle. Propagation parallel to the upstream magnetic field is along the vertical axis. The collisionless shock Friedrichs diagram depends sensitively upon the upstream C_S^2/C_A^2 , and this figure only illustrates the general behavior that is expected.

Volk et al., 1984]. They do not take into account any dependence of the superthermal "seed" particle injection rate on subshock parameters [Edmiston et al., 1982; J. P. Edmiston and C. F. Kennel, unpublished manuscript, 1984]. They overestimate the downstream cosmic ray pressure because they assume steady state, whereas ions only have time to diffuse to ~ 200 keV in the foreshocks of the bow shock and interplanetary shocks (H. Volk, personal communication, 1983). Nonetheless, they illustrate the relationship between the foreshock and subshock which will eventually be made more quantitative with a more refined theory.

Before we can arrive at a comprehensive theory that computes the energetic particle intensity and spectrum as a function of shock parameters, we must understand how particles that are originally part of the thermal plasma begin to be accelerated. Present energetic particle diffusion calculations start with a source of "seed" particles which can either be in the upstream flow or be injected at a subshock. It matters not for the final spectral index whether the seed particles are injected far upstream [Axford et al., 1977; Blandford and Ostriker, 1978] or at the subshock [Lee, 1982, 1983a]. However, the energetic particle intensity will depend upon the nature of

the source and therefore upon the shock normal angle as well as the Mach number. It now seems clear that seed particles are thermal ions that interact with the subshock once on their way to participating in the Fermi process. In the case of the bow shock, these are the few keV "upstream" ions that are reflected from or transmitted through the shock.

10.5. Supernova Shocks

The discoveries that most of the volume of the interstellar medium is in a hot low-density phase and that the composition of galactic cosmic rays is that of the interstellar medium and not of material recently processed in supernova explosions have revived the notion that supernova shocks Fermi accelerate the cosmic rays directly out of the interstellar medium. MHD shocks can produce the observed galactic cosmic ray energy spectrum. The density, temperature, and magnetic field in the hot interstellar medium are similar to those in the solar wind, and the Mach numbers of the supernova shocks at the phase when they accelerate the most cosmic rays are similar to those of solar system shocks. Thus, in addition to their intrinsic interest, studies of collisionless shocks in the solar system are directly relevant to the plasma physics of supernova shock acceleration.

11. Concluding Remarks

This review has focused on the critical Mach numbers at which collisionless shock structure changes. Figure 16, a Friedrichs diagram for collisionless shocks, summarizes, for $C_S^2 = 0.1 C_A^2$ upstream, the dependence upon the upstream shock normal angle of the first, second, and foreshock critical Mach numbers, and the ion sound resistive-dispersive transition for subcritical shocks. We assumed $T_{e2} = T_{i2}$ in computing the second and foreshock critical Mach numbers. The whistler critical Mach number and the critical Mach number discussed in section 10 are not shown. We hope that the use of such collisionless shock Friedrichs diagrams will facilitate rigorous studies of the dependence of shock structure upon upstream plasma parameters.

The staggering variety of collisionless shock structures predicted by theory and found in experiments over the past 25 years reflects the richness of contemporary plasma physics. Understanding collisionless shocks, the simplest of all nonlinear flow configurations, has required merging sophisticated concepts from nonlinear fluid physics with microscopic plasma physics, and, at all times, an exquisite sensitivity to parameter dependences. The next 25 years of collisionless shock research promise to be as fruitful as the past 25 years, as we extend our understanding to higher β and higher Mach number fast shocks, to slow shocks, and to relativistic shocks, and find further applications to the plasmas in the laboratory, at the sun and in the solar system, and in astrophysics.

Acknowledgments. We are pleased to acknowledge useful conversations with R. Blandford, E. Greenstadt, W. Livesey, M. Mellott, S. Moses, C. T. Russell, F. L. Scarf, and especially F. Coroniti. This work was supported by NASA NGL-05-007-190, NASA NSG 7341, and NSF ATM-81-19544.

References

- Anderson, K. A., Energetic electrons of terrestrial origin upstream in the solar wind, *J. Geophys. Res.*, **73**, 2387, 1968.
- Anderson, K. A., Energetic electrons of terrestrial origin behind the bow shock and upstream in the solar wind, *J. Geophys. Res.*, **74**, 95, 1969.
- Anderson, K. A., R. P. Lin, F. Martel, C. S. Lin, G. K. Parks, and H. Reme, Thin sheets of energetic electrons upstream from the Earth's bow shock, *Geophys. Res. Lett.*, **6**, 407, 1979.
- Anderson, R. R., G. K. Parks, T. E. Eastman, D. A. Gunnnett, and L. A. Frank, Plasma waves associated with energetic particles streaming into the solar wind from the Earth's bow shock, *J. Geophys. Res.*, **86**, 4493, 1981.
- Asbridge, J. R., S. J. Bame, and I. B. Strong, Outward flow of protons from the earth's bow shock, *J. Geophys. Res.*, **73**, 5777, 1968.
- Auer, P. L., R. W. Kilb, and W. H. Evers, Jr., Collision-free shock formation in finite temperature plasmas, *Phys. Fluids*, **14**, 1177, 1971.
- Auer, R. D., and H. J. Volk, Parallel high β shocks and relaxation phenomena, *Astrophys. Space Sci.*, **72**, 243, 1973.
- Axford, W. I., Acceleration of cosmic rays by shock waves, *Proc. Int. Conf. Cosmic Rays 17th*, **12**, 155, 1981.
- Axford, W. I., E. Leer, and G. Skadron, The acceleration of cosmic rays by shock waves, *Proc. Int. Conf. Cosmic Rays 15th*, **11**, 132, 1977.
- Axford, W. I., E. Leer, and J. F. McKenzie, The structure of cosmic ray shocks, *Astron. Astrophys.*, **111**, 317, 1982.
- Bame, S. J., J. R. Asbridge, J. T. Gosling, M. Halbig, G. Paschmann, N. Sckopke, and H. Rosenbauer, High temporal resolution observations of electron heating at the bow shock, *Space Sci. Rev.*, **23**, 75, 1979.
- Bame, S. J., J. R. Asbridge, W. C. Feldman, J. T. Gosling, G. Paschmann, and N. Sckopke, Deceleration of the solar wind upstream from the earth's bow shock and the origin of diffuse upstream ions, *J. Geophys. Res.*, **85**, 2981, 1980.
- Barnes, A., Theory of generation of bow-shock-associated hydromagnetic waves in the upstream interplanetary medium, *Cosmic Electrodyn.*, **1**, 90, 1970.
- Bekhtein, G. E., and R. Z. Sagdeev, Anomalous resistance of a plasma in the case of ion-acoustic turbulence (in Russian), *Zh. Eksp. Teor. Fiz. Pis'ma Red.*, **11**, 297, 1970. (*JETP Lett.*, Engl. Transl., **11**, 194, 1970.)
- Bekhtein, G. E., D. D. Ryutov, and R. Z. Sagdeev,

- Asymptotic solutions of the problem of the anomalous resistance of a collisionless plasma (in Russian), *Zh. Eksp. Teor. Fiz.*, 60, 2142, 1971. (*Sov. Phys. JETP*, Engl. Transl., 33, 1152, 1971.)
- Bell, A. R., The acceleration of cosmic rays in shock fronts, 1, *Mon. Not. R. Astron. Soc.*, 182, 147, 1978a.
- Bell, A. R., The acceleration of cosmic rays in shock fronts, 2, *Mon. Not. R. Astron. Soc.*, 182, 443, 1978b.
- Berezin, Yu. A., and R. Z. Sagdeev, One-dimensional nonlinear instability model for an anisotropic plasma, *Sov. Phys. Dokl.*, 14, 62, 1969.
- Biskamp, D., Collisionless shock waves in plasmas, *Nucl. Fusion*, 13, 719, 1973.
- Blandford, R. R., and J. P. Ostriker, Particle acceleration by astrophysical shocks, *Astrophys. J.*, 221, 129, 1978.
- Bonifazi, C., and G. Moreno, Reflected and diffuse ions backstreaming from the earth's bow shock, 1, Basic properties, *J. Geophys. Res.*, 86, 4397, 1981a.
- Bonifazi, C., and G. Moreno, Reflected and diffuse ions backstreaming from the earth's bow shock, 2, Origin, *J. Geophys. Res.*, 86, 4405, 1981b.
- Bonifazi, C., G. Moreno, A. J. Lazarus, and J. D. Sullivan, Deceleration of the solar wind in the earth's foreshock region: ISEE 2 and IMP 8 observations, *J. Geophys. Res.*, 85, 6031, 1980.
- Buneman, O., Dissipation of currents in ionized media, *Phys. Rev.*, 115, 503, 1959.
- Chen, G., and T. P. Armstrong, Particle acceleration in the interplanetary medium, 1, Numerical simulation of the motions of charged particles near interplanetary shock waves, paper presented at Panel Presentation 5 of the Conference on Solar Terrestrial Relations, Calgary, Alberta, Aug. 28 to Sept. 1, 1972.
- Chodura, R., A hybrid fluid particle model of ion heating in high Mach-number shock waves, *Nucl. Fusion*, 15, 55, 1975.
- Coroniti, F. V., Dissipation discontinuities in hydromagnetic shock waves, *J. Plasma Phys.*, 4, 265, 1970.
- Coroniti, F. V., Laminar wave-train structure of collisionless magnetic slow shocks, *Nucl. Fusion*, 11, 261, 1971.
- DeHoffman, F., and E. Teller, Magnetohydrodynamic shocks, *Phys. Rev.*, 80, 692, 1950.
- Drury, L., and H. J. Volk, Hydromagnetic shock structure in the presence of cosmic rays, *Astrophys. J.*, 248, 344, 1981.
- Dum, C. T., Anomalous heating by ion sound turbulence, *Phys. Fluids*, 21, 945, 1978a.
- Dum, C. T., Anomalous electron transport equations for ion sound and related turbulent spectra, *Phys. Fluids*, 21, 956, 1978b.
- Eastman, T. E., R. R. Anderson, L. A. Frank, and G. K. Parks, Upstream particles observed in the earth's foreshock region, *J. Geophys. Res.*, 86, 4379, 1981.
- Edmiston, J. P., and C. F. Kennel, A parametric survey of the first critical Mach number for a fast MHD shock, *J. Plasma Phys.*, 32, 429, 1984.
- Edmiston, J. P., C. F. Kennel, and D. Eichler, Escape of heated ions upstream of quasi-parallel shocks, *Geophys. Res. Lett.*, 9, 531, 1982.
- Eichler, D., Particle acceleration in collisionless shocks: Regulated injection and high efficiency, *Astrophys. J.*, 229, 419, 1979.
- Eichler, D., Energetic particle spectra in finite shocks: The earth's bow shock, *Astrophys. J.*, 244, 711, 1981.
- Ellison, D. C., Monte Carlo simulations of charged particles upstream of the earth's bowshock, *Geophys. Res. Lett.*, 8, 991, 1981.
- Eselevich, V. G., Shock-wave structure in collisionless plasmas from results of laboratory experiments, *Space Sci. Rev.*, 32, 65, 1982.
- Eselevich, V. G., Bowshock structure from laboratory and satellite experimental results, *Planet. Space Sci.*, 31, 615, 1983.
- Eselevich, V. G., A. G. Eskov, R. Kh. Kurtmullaev, and A. I. Malyutin, Isomagnetic discontinuity in a collisionless shock, *Sov. Phys. JETP*, Engl. Transl., 33, 1120, 1971.
- Etcheto, J., and M. Faucheux, Detailed study of electron plasma waves upstream of the earth's bowshock, *J. Geophys. Res.*, 89, 6631, 1984.
- Fairfield, D. H., Bowshock associated waves observed in the far upstream interplanetary medium, *J. Geophys. Res.*, 74, 3541, 1969.
- Fairfield, D. H., Whistler waves observed upstream from collisionless shock, *J. Geophys. Res.*, 79, 1368, 1974.
- Feldman, W. C., J. R. Asbridge, S. J. Bame, and M. D. Montgomery, Solar wind heat transport in the vicinity of the earth's bow shock, *J. Geophys. Res.*, 78, 3697, 1973.
- Feldman, W. C., R. C. Anderson, S. J. Bame, S. P. Gary, J. T. Gosling, D. J. McComas, M. F. Thomsen, G. Paschmann, and M. M. Hoppe, Electron velocity distributions near the earth's bow shock, *J. Geophys. Res.*, 88, 96, 1983.
- Fisk, L. A., Increases in the low-energy cosmic ray intensity at the front of propagating interplanetary shock waves, *J. Geophys. Res.*, 76, 1662, 1971.
- Forman, M. A., Acceleration theory for 5-40 keV ions at interplanetary shocks, *Adv. Space Res.*, 1, 3, 97, 1981.
- Formisano, V., The physics of the earth's collisionless shock wave, *J. Phys.*, 38, C6-55-C6-88, 1977.
- Formisano, V., and P. Hedgecock, Solar wind interaction with the earth's magnetic field, 3, On the earth's bowshock structure, *J. Geophys. Res.*, 78, 3745, 1973a.
- Formisano, V., and P. Hedgecock, On the structure of the turbulent bowshock, *J. Geophys. Res.*, 78, 6522, 1973b.
- Formisano, V., and C. F. Kennel, Small amplitude waves in high β plasmas, *J. Plasma Phys.*, 3, 55, 1969.
- Forslund, D. W., K. B. Quest, J. V. Brackbill, and K. Lee, Collisionless dissipation in quasi-perpendicular shocks, *J. Geophys. Res.*, 89, 2142, 1984.
- Fredericks, R. W., and C. F. Kennel, Magnetosonic wave propagating across a magnetic field in a collisionless plasma, *J. Geophys. Res.*, 73, 7429, 1968.
- Fuselier, S. A., and D. A. Gurnett, Short wavelengths ion waves upstream of the earth's bow shock, *J. Geophys. Res.*, 89, 91, 1984.
- Galeev, A. A., Collisionless shocks, in *Physics of Solar Planetary Environment*, edited by D. J. Williams, p. 464, AGU, Washington, D. C., 1976.
- Galeev, A. A., and V. I. Karpman, Turbulence theory of a weakly nonequilibrium low density plasma and structure of shock waves, *Sov. Phys. JETP*, Engl. Transl., 17, 403, 1963.
- Galeev, A. A., and R. Z. Sagdeev, Model of a shock wave in solar wind plasma, *Sov. Phys. JETP*, Engl. Transl., 30, 571, 1970.
- Gary, S. P., Microinstabilities upstream of the earth's bowshock: A brief review, *J. Geophys. Res.*, 86, 4331, 1981.
- Gary, S. P., J. T. Gosling, and D. W. Forslund, The electromagnetic ion beam instability upstream of the earth's bowshock, *J. Geophys. Res.*, 86, 6691, 1981.
- Gosling, J. T., J. R. Asbridge, S. J. Bame, G. Paschmann, and N. Sckopke, Observations of two distinct populations of bow shock ions, *Geophys. Res. Lett.*, 5, 957, 1978.
- Gosling, J. T., J. R. Asbridge, S. J. Bame, W. C. Feldman, G. Paschmann, and N. Sckopke, Solar wind ions accelerated to 40 keV by shock wave disturbances, *J. Geophys. Res.*, 85, 744, 1980.
- Gosling, J. T., J. R. Asbridge, S. J. Bame, W. C. Feldman, R. B. Zwickl, G. Paschmann, N. Sckopke, and R. J. Hynds, Interplanetary ions during an energetic storm particle event: The distribution function from solar wind thermal energies to 1.6 MeV, *J. Geophys. Res.*, 86, 547, 1981.
- Gosling, J. T., M. F. Thomsen, S. J. Bame, and W. C. Feldman, Evidence for specularly reflected ions upstream from the quasi-parallel bowshock, *Geophys. Res. Lett.*, 9, 1333, 1982.
- Gosling, J. T., S. J. Bame, and W. C. Feldman, Low energy ($E \lesssim 30$ keV) suprathermal ions upstream from interplanetary shocks (abstract), *Solar Wind Five, NASA Conf. Publ.*, CP2280, 401, 1983.
- Gosling, J. T., S. J. Bame, W. C. Feldman, G. Paschmann, N. Sckopke, and C. T. Russell, Suprathermal ions upstream from interplanetary shocks, *J. Geophys. Res.*, 89, 5409, 1984.
- Greenstadt, E. W., The upstream escape of energized solar wind protons from the bowshock, in *The Magnetospheres of Earth and Jupiter*, edited by V. Formisano, D. Reidel, Hingham, Mass., 1975.
- Greenstadt, E. W., Phenomenology of the earth's bow shock system, a summary description, in *Magnetospheric Particles and Fields*, edited by B. M. McCormac, p. 13, D. Reidel, Hingham, Mass., 1976a.
- Greenstadt, E. W., Energies of backstreaming protons in the foreshock, *Geophys. Res. Lett.*, 3, 553, 1976b.
- Greenstadt, E. W., Oblique, parallel, and quasi-parallel morphology of collisionless shocks, this volume.
- Greenstadt, E. W., and R. W. Fredricks, Shock systems in collisionless space plasmas, in *Solar System Plasma Physics*, vol. III, edited by L. J. Lanzerotti, C. F. Kennel, and E. N. Parker, p. 3, North-Holland, Amsterdam, 1979.
- Greenstadt, E. W., I. M. Green, G. T. Inouye, A. J. Hundhausen, S. J. Bame, and I. B. Strong, Correlated magnetic field and plasma observations of the earth's bow shock, *J. Geophys. Res.*, 73, 51, 1968.
- Greenstadt, E. W., I. M. Green, G. T. Inouye, D. S. Colburn, J. H. Binsack, and E. F. Lyon, Dual satellite observation of the Earth's bowshock, 1, The thick pulsation shock, 2, Field-aligned upstream waves, 3, Field-determined shock structure, *Cosmic Electrodynamic.*, 1, 279, 1970.
- Greenstadt, E. W., M. Hoppe, and C. T. Russell, Magnetic field orientation and suprathermal ion streams in the earth's foreshock, *J. Geophys. Res.*, 85, 3473, 1980.
- Greenstadt, E. W., V. Formisano, C. Goodrich, J. T. Gosling, M. Lee, M. Leroy, M. Mellott, K. Quest, A. E. Robson, P. Rodriguez, J. Scudder, J. Slavin, M. Thomsen, D. Winske, and C. S. Wu, Collisionless shock waves in the solar terrestrial environment, in *Solar-Terrestrial Physics: Past and Future, NASA Ref. Publ.* 1120, p. 424, 1984.
- Gurgiolo, C., G. K. Parks, B. H. Mauk, C. S. Lin, K. A. Anderson, R. P. Lin, and H. Reme, Non $E \times B$ ordered ion beams upstream of the earth's bowshock, *J. Geophys. Res.*, 86, 4415, 1981.
- Hada, T., and C. F. Kennel, Nonlinear evolution of slow waves in the solar wind, *J. Geophys. Res.*, 90, 531, 1985.
- Hoppe, M., C. T. Russell, L. A. Frank, T. E. Eastman, and E. W. Greenstadt, Upstream hydromagnetic waves and their association with backstreaming ion populations: ISEE 1 and 2 observations, *J. Geophys. Res.*, 86, 4471, 1981.
- Hoppe, M. M., C. T. Russell, T. E. Eastman, and L. A. Frank, Characteristics of the ULF waves associated with upstream ion beams, *J. Geophys. Res.*, 87, 643, 1982.
- Ipavich, F. M., A. B. Galvin, G. Gloeckler, M. Scholger, and D. Hovestadt, A statistical survey of ions observed upstream of the earth's bowshock: Spectra, composition, and spatial variation, *J. Geophys. Res.*, 86, 4337, 1981a.
- Ipavich, F. M., M. Scholger, and G. Gloeckler, Temporal development of composition, spectra, and anisotropies during upstream particle events, *J. Geophys. Res.*, 86, 11,153, 1981b.
- Jackson, R. W., Second-order effects related to a model for a parallel shock, *J. Geophys. Res.*, 88, 9981, 1983.
- Kan, J. R., and D. W. Swift, Structure of quasi-parallel bowshock: Results of numerical simulations, *J. Geophys. Res.*, 88, 6919, 1983.
- Kantrowitz, A. R., and H. E. Petschek, MHD characteristics and shock waves, in *Plasma Physics in Theory and Application*, edited by W. B. Kunkel, p. 148, McGraw-Hill, New York, 1966.
- Karpman, V. I., Structure of the shock front propagating

- at an angle of the magnetic field in a low density plasma, *Sov. Phys. Tech. Phys.*, Engl. Transl., **8**, 715, 1964.
- Keilhacker, M., M. Kornherr, H. Niedermeyer, K. H. Steuer, and R. Chodura, Experimental study of collective dissipation of shock waves for a wide range of plasma parameters, in *Plasma Physics and Controlled Nuclear Fusion Research 1171*, vol. 3, p. 265, International Atomic Energy Agency, Vienna, 1972.
- Kennel, C. F., and H. E. Petschek, Magnetic turbulence in shocks, in *Physics of the Magnetosphere*, edited by R. Carovillano, J. F. McClay, and H. R. Radoski, p. 485, D. Reidel, Hingham, Mass., 1968.
- Kennel, C. F., and R. Z. Sagdeev, Collisionless shock waves in high plasmas, **1**, *J. Geophys. Res.*, **72**, 3303, 1967.
- Kennel, C. F., and F. L. Scarf, Thermal anisotropies and electromagnetic instabilities in the solar wind, *J. Geophys. Res.*, **73**, 6149, 1968.
- Kennel, C. F., F. L. Scarf, F. V. Coroniti, E. J. Smith, and D. A. Gurnett, Nonlocal plasma turbulence associated with interplanetary shocks, *J. Geophys. Res.*, **87**, 1774, 1982.
- Kennel, C. F., F. L. Scarf, F. V. Coroniti, C. T. Russell, K. P. Wenzel, T. R. Sanderson, P. Van Nes, W. C. Feldman, G. K. Parks, E. J. Smith, B. T. Tsurutani, F. S. Mozer, M. Temerin, R. R. Anderson, J. D. Scudder, and M. Scholer, Plasma and energetic particle structure upstream of a quasi-parallel interplanetary shock, *J. Geophys. Res.*, **89**, 5419, 1984a.
- Kennel, C. F., J. P. Edmiston, F. L. Scarf, F. V. Coroniti, C. T. Russell, E. J. Smith, B. T. Tsurutani, J. D. Scudder, W. C. Feldman, R. R. Anderson, F. S. Moser, and M. Temerin, Structure at the November 12, 1978, quasi-parallel interplanetary shock, *J. Geophys. Res.*, **89**, 5436, 1984b.
- Klecker, B., M. Scholer, D. Hovestadt, G. Gloeckler, and F. M. Ipavich, Spectral and compositional variations of low energy ions during an energetic storm particle event, *Astrophys. J.*, **251**, 393, 1981.
- Krimsky, G. F., A regular mechanism for the acceleration of charged particles on the front of a shock wave (in Russian), *Dokl. Akad. Nauk SSSR*, **234**, 1306, 1977.
- Lee, M. A., Coupled hydromagnetic waves excitation and ion acceleration upstream of the earth's bow shock, *J. Geophys. Res.*, **87**, 5063, 1982.
- Lee, M. A., Coupled hydromagnetic wave excitation and ion acceleration at interplanetary traveling shocks, *J. Geophys. Res.*, **88**, 6109, 1983a.
- Lee, M. A., The association of energetic particles and shocks in the heliosphere, *Rev. Geophys. Space Phys.*, **21**, 324, 1983b.
- Lee, M. A., and L. Fisk, Shock acceleration of energetic particles in the heliosphere, *Space Sci. Rev.*, **32**, 205, 1982.
- Lee, M. A., G. Skadron, and L. A. Fisk, Acceleration of energetic ions at the earth's bowshock, *Geophys. Res. Lett.*, **8**, 401, 1981.
- Lemons, D. A., and S. P. Gary, Current-driven instabilities in a laminar perpendicular shock, *J. Geophys. Res.*, **83**, 1625, 1978.
- Leroy, M. M., Structure of perpendicular shocks in collisionless plasma, *Phys. Fluids*, **26**, 2742, 1983.
- Leroy, M. M., and D. Winske, Backstreaming ions from oblique earth bow shocks, *Ann. Geophys.*, **1**, 527, 1983.
- Leroy, M. M., C. C. Goodrich, D. Winske, C. S. Wu, and K. Papadopoulos, Simulations of perpendicular bow shock, *Geophys. Res. Lett.*, **8**, 1269, 1981.
- Leroy, M. M., D. Winske, C. C. Goodrich, C. S. Wu, and K. Papadopoulos, The structure of perpendicular bowshocks, *J. Geophys. Res.*, **87**, 5081, 1982.
- Levy, R. H., H. E. Petschek, and G. L. Siscoe, Aerodynamic aspects of the magnetospheric flow, *AIAA J.*, **2**, 2065, 1964.
- Lin, R. P., C. I. Meng, and K. A. Anderson, 30-to-100 keV protons upstream of the earth's bowshock, *J. Geophys. Res.*, **79**, 489, 1974.
- Livesey, W. A., C. F. Kennel, and C. T. Russell, ISEE 1 and 2 observations of magnetic field strength overshoots in quasi-perpendicular bowshocks, *Geophys. Res. Lett.*, **9**, 1037, 1982.
- Livesey, W. A., C. T. Russell, and C. F. Kennel, A comparison of specularly reflected gyrating ion orbits with observed shock foot thicknesses, *J. Geophys. Res.*, **89**, 6824, 1984.
- Manheimer, W. M., and D. S. Spicer, Longitudinal resistivity and intermediate Mach number collisionless transverse magnetosonic shocks, *Phys. Fluids*, in press, 1985.
- Marshall, W., The structure of magnetohydrodynamic shock waves, *Proc. R. Soc. London, Ser. A*, **233**, 367, 1955.
- McKenzie, J. F., and H. J. Volk, Nonlinear theory of cosmic ray shocks including self-generated Alfvén waves, *Astron. Astrophys.*, **116**, 191, 1982.
- Mellott, M. M., and E. W. Greenstadt, ISEE 1 and 2 observations of laminar bow shocks: Whistler precursors and shock structure, *J. Geophys. Res.*, **89**, 2151, 1984.
- Mitchell, D. G., and E. Roelof, Dependence of 50-keV upstream ion events at IMP 7 and 8 upon magnetic field bow shock geometry, *J. Geophys. Res.*, **88**, 5623, 1983.
- Moiseev, S. S., and R. Z. Sagdeev, Collisionless shock waves in a plasma in a weak magnetic field, in *Plasma Phys. J. Nucl. Energy, Part C*, **5**, 43, 1963.
- Montgomery, M. D., J. R. Asbridge, and S. J. Bame, Vela 4 plasma observations near the earth's bowshock, *J. Geophys. Res.*, **75**, 1217, 1970.
- Ness, N. F., C. S. Scarse, and J. B. Seek, Initial results of the IMP 1 magnetic field experiment, *J. Geophys. Res.*, **69**, 3531, 1964.
- Papadopoulos, K., Comments on high Mach number magnetosonic shock, in *Plasma Astrophysics, ESA SP-161*, edited by T. D. Guyenn and G. Levy, p. 409, European Space Agency, Neuilly, France, 1981a.
- Papadopoulos, K., Electron acceleration in magnetosonic shock fronts, in *Plasma Astrophysics, ESA SP-161*, edited by T. D. Guyenn and G. Levy, p. 313, European Space Agency, Neuilly, France, 1981b.
- Parker, E. N., A quasi-linear model of plasma shock structure in a longitudinal magnetic field, *J. Nucl. Energy, C2*, **146**, 1961.
- Parks, G. K., E. Greenstadt, C. S. Wu, C. S. Lin, A. St-Marc, R. P. Lin, K. A. Anderson, C. Gurgiolo, B. Mauk, R. Anderson, and T. Eastman, Upstream particle spatial gradients and plasma waves, *J. Geophys. Res.*, **86**, 4343, 1981.
- Paschmann, G., N. Sckopke, S. J. Bame, J. R. Asbridge, J. T. Gosling, C. T. Russell, and E. W. Greenstadt, Association of low-frequency waves with suprathermal ions in the upstream solar wind, *Geophys. Res. Lett.*, **6**, 209, 1979.
- Paschmann, G., N. Sckopke, I. Papamastorakis, J. R. Asbridge, S. J. Bame, and J. T. Gosling, Characteristics of reflected and diffuse ions upstream from the earth's bowshock, *J. Geophys. Res.*, **86**, 4355, 1981.
- Paschmann, G., N. Sckopke, S. J. Bame, and J. T. Gosling, Observations of gyrating ions in the foot of a nearly perpendicular bowshock, *Geophys. Res. Lett.*, **9**, 881, 1982.
- Paul, J. W. M., L. A. Holmes, J. J. Parkinson, and J. Sheffield, Experimental observations on the structure of collisionless shock waves in a magnetized plasma, *Nature*, **208**, 133, 1965.
- Paul, J. W. M., G. C. Goldenbaum, A. Ioyashi, L. S. Holmes, and R. A. Hardcastle, Measurements of electron temperatures produced by collisionless shock waves in magnetized plasma, *Nature*, **216**, 363, 1967.
- Pesses, M. E., On the acceleration of energetic protons by interplanetary shock waves, Ph.D. thesis, Univ. of Iowa, Iowa City, 1979.
- Petschek, H. E., Aerodynamic dissipation, *Rev. Mod. Phys.*, **30**, 966, 1958.
- Phillips, P. E., and A. E. Robson, Influence of reflected ions on the magnetic structure of a collisionless shock front, *Phys. Rev. Lett.*, **29**, 154, 1972.
- Quest, K. B., D. W. Forslund, J. U. Brackbill, and K. Lee, Collisionless dissipation processes in quasi-parallel shocks, *Geophys. Res. Lett.*, **10**, 471, 1983.
- Rodriguez, P., and D. A. Gurnett, Electrostatic and electromagnetic turbulence associated with the earth's bowshock, *J. Geophys. Res.*, **80**, 19, 1975.
- Russell, C. T., E. J. Smith, B. T. Tsurutani, J. T. Gosling, and S. J. Bame, Multiple spacecraft observations of interplanetary shocks: Characteristics of the upstream ULF turbulence, Solar Wind Fire, *NASA Conf. Publ.*, **CP2280**, 385, 1983.
- Sagdeev, R. Z., Cooperative phenomena and shock waves in collisionless plasma, *Rev. Plasma Phys.*, Engl. Transl., **4**, 23, 1966.
- Sagdeev, R. Z., The 1976 Oppenheimer lectures: Critical problems in plasma astrophysics, II, Singular layers and reconnection, *Rev. Mod. Phys.*, **51**, 11, 1979.
- Sagdeev, R. Z., and A. A. Galeev, *Nonlinear Plasma Theory*, W. A. Benjamin, Reading, Mass., 1969.
- Sarris, E. T., and R. Reinhard, Fine-time scale multi-spacecraft observations of the May 17, 1971 storm particle event, in *Solar Wind Four*, edited by H. Rosenbauer, p. 503, Springer-Verlag, New York, 1981.
- Scarf, F. L., R. W. Fredricks, L. A. Frank, C. T. Russell, P. J. Coleman, Jr., and M. Neugebauer, Direct correlations of large-amplitude waves with suprathermal protons in the upstream solar wind, *J. Geophys. Res.*, **75**, 7316, 1970.
- Scarf, F. L., R. W. Fredricks, L. A. Frank, and M. Neugebauer, Nonthermal electrons and high-frequency waves in the upstream solar wind, **1**, Observations, *J. Geophys. Res.*, **76**, 5162, 1971.
- Scholer, M., and G. Morfill, Simulation of solar flare particle interaction with interplanetary shock waves, *Sol. Phys.*, **45**, 227, 1975.
- Scholer, M., F. M. Ipavich, G. Gloeckler, D. Hovestadt, and B. Klecker, Pitch angle distributions of energetic protons near the earth's bowshock, *Geophys. Res. Lett.*, **6**, 707, 1979.
- Scholer, M., F. M. Ipavich, G. Gloeckler, and D. Hovestadt, Acceleration of low-energy protons and alpha particles at interplanetary shock waves, *J. Geophys. Res.*, **88**, 1977, 1983.
- Schwartz, S. J., M. F. Thomsen, and J. T. Gosling, Ions upstream of the earth's bowshock: A theoretical comparison of alternative source populations, *J. Geophys. Res.*, **88**, 2039, 1983.
- Sckopke, N., G. Paschmann, S. J. Bame, J. T. Gosling, and C. T. Russell, Evolution of ion distributions across the nearly perpendicular bow shock, *J. Geophys. Res.*, **88**, 6121, 1983.
- Segre, S. E., and M. Martone, Measurements on the heating in collisionless, low β transverse shock waves near the critical Alfvén Mach number, *Plasma Phys.*, **13**, 113, 1971.
- Sentman, D. D., C. F. Kennel, and L. A. Frank, Plasma rest-frame distributions of suprathermal ions in the earth's foreshock region, *J. Geophys. Res.*, **86**, 4365, 1981a.
- Sentman, D. D., J. P. Edmiston, and L. A. Frank, Instabilities of low-frequency, parallel propagating electromagnetic waves in the earth's foreshock region, *J. Geophys. Res.*, **86**, 7487, 1981b.
- Sentman, D. D., M. F. Thomsen, S. P. Gary, W. C. Feldman, and M. M. Hoppe, The oblique whistler instability in the earth's foreshock, *J. Geophys. Res.*, **88**, 2048, 1983.
- Shabanskii, V. P., Particle acceleration by passage of a hydromagnetic shock wave front, *Sov. Phys. JETP*, Engl. Transl., **14**, 791, 1962.
- Skadron, G., and M. A. Lee, The two-dimensional structure of diffuse ions associated with the earth's bow shock, *Astrophys. J.*, **468**, 1982.
- Sonett, C. P., and I. J. Abrams, The distant geomagnetic field, **3**, Disorder and shocks in the magnetopause, *J. Geophys. Res.*, **68**, 1233, 1963.
- Sonnerup, B. U. O., Acceleration of particles reflected at a shock front, *J. Geophys. Res.*, **74**, 1301, 1969.
- Stringer, T. E., Low-frequency waves in an unbounded plasma, *Plasma Phys. J. Nucl. Energy, Part C*, **5**, 89, 1963.

- Tanaka, M., C. C. Goodrich, D. Winske, K. Papadopoulos, A source of the backstreaming ion beams in the foreshock region, *J. Geophys. Res.*, **88**, 3046, 1983.
- Terasawa, T., Energy spectrum and pitch angle distribution of particles reflected by MHD shock waves of fast mode, *Planet. Space Sci.*, **27**, 193, 1979a.
- Terasawa, T., Origin of 30–100 keV protons observed in the upstream region of the earth's bow shock, *Planet. Space Sci.*, **27**, 365, 1979b.
- Terasawa, T., Energy spectrum of ions accelerated through Fermi process at the terrestrial bow shock, *J. Geophys. Res.*, **86**, 7595, 1981.
- Tidman, D. A., and N. A. Krall, *Shock Waves in Collisionless Plasmas*, p. 166, Wiley-Interscience, New York, 1971.
- Tokar, R. L., D. A. Gurnett, and W. C. Feldman, Whistler mode turbulence generated by electron beams in earth's bow shock, *J. Geophys. Res.*, **89**, 105, 1984.
- Tsurutani, B. T., and R. P. Lin, Acceleration of >47 keV ions and >2keV electrons by interplanetary shocks at 1 AU, *J. Geophys. Res.*, **90**, 1, 1985.
- Tsurutani, B. T., and P. Rodriguez, Upstream waves and particles: An overview of ISEE results, *J. Geophys. Res.*, **86**, 4319, 1981.
- Tsurutani, B. T., E. J. Smith, and D. E. Jones, Waves observed upstream of interplanetary shocks, *J. Geophys. Res.*, **88**, 5645, 1983.
- Van Nes, P., R. Reinhard, T. R. Sanderson, K. P. Wenzel, and R. D. Zwickl, The energy spectrum of 35–1600 keV protons associated with interplanetary shocks, *J. Geophys. Res.*, **89**, 2122, 1984.
- Vinas, A. F., M. L. Goldstein, and M. H. Acuna, Spectral analysis of magnetohydrodynamic fluctuations near interplanetary shocks, *J. Geophys. Res.*, **89**, 3762, 1984.
- Volk, H. J., L. O'C. Drury, and J. F. McKenzie, Hydrodynamic estimates of cosmic ray acceleration efficiencies in shock waves, *Astron. Astrophys.*, **130**, 19, 1984.
- Wentzel, D. G., High speed interstellar gas dynamics: Shocks moderated by cosmic rays, *Astrophys. J.*, **170**, 53, 1971.
- Winske, D., Microtheory of collisionless shock current layers, this volume.
- Woods, L. C., On the structure of collisionless magnetoplasma shock waves at supercritical Alfvén-Mach numbers, *J. Plasma Phys.*, **3**, 435, 1969.
- Woods, L. C., On double structured, perpendicular, magneto-plasma shock waves, *J. Plasma Phys.*, **13**, 281, 1971.
- Wu, C. S., D. Winske, Y. M. Zhou, S. T. Tsai, P. Rodriguez, M. Tanaka, K. Papadopoulos, K. Akimoto, C. S. Lin, M. M. Leroy, and C. C. Goodrich, Microinstabilities associated with a high Mach-number, perpendicular shock, *Space Sci. Rev.*, **37**, 65, 1984.

Some Macroscopic Properties of Shock Waves in the Heliosphere

A. J. HUNDHAUSEN

High Altitude Observatory, National Center for Atmospheric Research, Boulder, Colorado 80307

In situ plasma and magnetic field observations demonstrate the existence of collisionless shocks associated with spatial inhomogeneities or temporal variations in the solar wind and with solar wind-planetary interactions. Remote observations suggest that similar shocks occur in association with solar activity in the solar corona. This tutorial will be focused on the formation and propagation of such shock waves in the heliospheric plasma. I will draw upon simple theoretical models (both analytic and numerical) of these phenomena to illuminate the basic physical processes controlling shock formation and propagation in the interplanetary medium.

1. Introduction

Kennel [this volume] describes physical processes that can account for the existence of shock fronts in plasmas where Coulomb collisions are extremely rare. The thickness of such a collisionless shock (or more precisely, the spatial scale over which the entropy of plasma flowing through the shock front is increased) depends upon the detailed nature of those processes. From a macroscopic point of view, in which the plasma flow in a physical system is considered on a spatial scale much larger than the thickness of any shocks it may contain, these details are unimportant. Such a flow can be described using the methods of fluid dynamics or magnetohydrodynamics without specific knowledge of, or reference to, the actual nature of the shock mechanism. The physical properties of the plasma on the two sides of the shock "layer" can be related by mass, momentum, energy, and magnetic conservation laws to yield the well-known [e.g., *Colburn and Sonett*, 1966; *Burlaga*, 1971] Rankine-Hugoniot relations.

The existence of collisionless shocks was first suggested as an explanation of the sudden commencement of some geomagnetic storms; a shock was postulated at the leading edge of a plasma cloud ejected from the sun by a solar flare [*Gold*, 1955] despite the objection that the material in interplanetary space must be so tenuous that ordinary Coulomb collision lengths were astronomically large. Interplanetary observations have since confirmed the existence of such shock waves propagating outward through the solar wind. These observations have also revealed the existence of large-amplitude variations in

solar wind speed that correspond to the "corotating streams" suggested by other studies of geomagnetic activity. These streams are usually not preceded by shocks near the orbit of earth but are observed to steepen and form shock fronts farther out in the solar system. Thus nature affords us, in the solar wind, the opportunity to study both the formation and propagation of shocks in a natural, collisionless plasma. These two aspects of macroscopic or large-scale shock behavior will be the foci of this paper. This emphasis will lead to neglect of several other interesting shock phenomena stemming from the interaction of the supersonic solar wind with obstacles in its flow: for example, planetary or cometary bow shocks and the termination of the solar wind through its interaction with the interstellar medium. Discussion of these phenomena can be found elsewhere in this volume [*Spreiter and Stahara*, this volume] and in the work by *Axford* [1972].

The tone of this exposition will be "tutorial." Shock phenomena are inherently complicated, and I have often heard it said that those who have not worked extensively with shock waves have little intuitive understanding of their behavior. Of course, much of the intuition we have for complicated physical phenomena is "educated intuition" based on the study of idealized examples that illustrate general behavior and lead to the capability of "guessing accurately" the behavior of real, physical systems. I will attempt to follow this path by illustrating the formation and propagation of shock waves in the heliosphere through examples based on the simplest possible quantitative model that contains the physics basic to